

Ground Truthing Earth's Silicate Weathering Thermostat: Using the Geochemistry of Himalayan Groundwaters to Calculate Residence Times

Giovanni Bernardi

Part III Project

2024-2025



Abstract

IMO, the abstract should be a supercondensed version of the paper.

Grab the readers attention -> why we care about the topic

What's the unknown? Are fluids actually following the Maher model?

How did you do this? Collected samples, tested models.

What did you find? The Maher model isn't appropriate etc

Loop back into the original part about why we care and the unknown. Has it been answered? What are the implications?

Residence time calculations determined using rate constants close to equilibrium give ages of order ten years for the model which purports discharge to be the greatest control on weathering. The other model, following the null hypothesis that temperature is the greatest control on weathering, gives residence times of a similar order of magnitude but the assumption of a constant rate of reaction is likely unrealistic. Simple calculations based on yearly rainfall support the residence time obtained by both models. Estimates of free energy suggest that the weathering reactions contributing to the dissolved load in the groundwater are not close to equilibrium. As a result, it is unlikely that the fast rates of reaction used are appropriate for catchments like Melamchi. Furthermore, this suggests that the main assumption of the Maher model is not valid in this catchment. These analyses suggest that a combination of both models' is necessary to accurately model a real catchment like Melamchi.

Contents

Abstract	i
1 Introduction	1
2 Study Area	7
2.1 Geology and Geomorphic Setting	7
2.2 Climate	7
3 Data Collection and Measurement	10
3.1 Field Sampling	10
3.2 Major and Trace Element Analysis	10
4 Methods and Models for Analysis	10
4.1 Rain and Hydrothermal Correction	10
4.2 Identifying the Weathering Reaction	11
4.3 One-Dimensional Reactive Transport Models	13
4.4 Estimates of Uncertainty	21
5 Results: Spring Chemistry and Residence Time	22
5.1 Traverse 1	22
5.2 Traverse 2	23
5.3 Traverse 3	24
5.4 Traverse 4	25
5.5 Traverse 5	26
5.6 Time Series Trends	27
6 Discussion	28

6.1	Explaining Traversal Variations in Chemistry	28
6.2	Residence Time Agreement with Gas Ages	29
6.3	Free Energy Calculations suggest Far From Equilibrium System	30
6.4	Model Pitfalls	32
6.5	Significance of Free Energy for Reaction Rate	35
7	Conclusions and Future Work	37
References		38
Appendix 1: Rain and Hydrothermal Correction Equations		46
Appendix 2: Derivation of Reactive Transport Models		48

Acknowledgements

This thesis would not have been possible without the amazing help from my supervisor, Ed Tipper. Mike Bickle and Al Knight and Morag Hunter have also been instrumental in guiding me through this Master's year. To Zara, I couldn't ask for a better field partner. To my friends and peers, thank you for supporting me throughout. A Mamma, Papà, e la Virgi, grazie di tutto come sempre. And finally, Beth,

List of Figures

- Figure 1:
- Figure 2:
- Figure 3:
- Figure 4:
- Figure 5:
- Figure 6:
- Figure 7:
- Figure 8:
- Figure 9:
- Figure 10:
- Figure 11:

List of Tables

- Table 1:
- Table 2:
- Table 3:
- Table 4:
- Table 5:
- Table 6:
- Table 7:

Nomenclature

- Kinetically limited
- Chemical Equilibrium
- Reactive Transport Model
- Runoff
- Discharge
- Fontorbe Model
- Maher model
- Residence time
- Flow Path Length
- Porosity
- HHCS
- LHS
- MCT
- ISM
- Lapse Rate
- Modal Decomposition
- Free Energy
- DSi

1 Introduction

Silicate weathering, whereby silicate minerals are dissolved by carbonic acid, sequesters atmospheric CO₂ over long (10⁶ year) timescales, and is proposed to be the dominant mechanism by which global climate is controlled on multi-million year timescales. As water passes through the subsurface, it interacts with the surrounding rock. This causes the addition of solute species to the groundwater, and the formation of stable secondary minerals through the dissolution of primary minerals. Large mountain ranges in particular are thought to be most sensitive to weathering (Tipper et al., 2006). The Himalayan mountain range spans more than 590,000 km², and is the source of major rivers, including the Ganges, Brahmaputra, and Indus. Silicate weathering in the Himalayas as a result of their uplift and erosion in the Cenozoic may have contributed significantly to the global cooling over the past 40 million years (Raymo and Ruddiman, 1992; West et al, 2005, Kump et al, 2000). Clearly, understanding the strongest control on weathering in these key regions for the global carbon cycle is of utmost importance to inform climate policy.

The dissolution kinetics of the silicate rocks in Himalayan catchments are thought to be sensitive to temperature and runoff because the weathering reactions have not gone to completion. Weathering regimes can be classified as either transport-limited or kinetically limited (West et al., 2005). West et al. (2005) distinguish the two regimes by the rate of erosion in the catchment. In low erosion rate settings, weathering is transport-limited due to limited mineral supply. Here, weathering rate is proportional to the material eroded. In high erosion rate settings, there is an abundant mineral supply and so only kinetics stand in the way of the weathering reaction. Rapidly eroding catchments like Melamchi are likely kinetically-limited (Stallard & Edmund 1983 JGR, West et al, 2005). In highly erosive regions like Melamchi, silicate weathering reactions are thought to be more sensitive to temperature than runoff. Soil properties and topography are also linked to weathering regimes in the subsurface (Pedrazas et al, 2021). Indeed, bedrock strength is thought to be more dependent on weathering than mineral or textural differences between the metamorphic lithologies in the Himalayas (Medwedeff et al, 2021). Therefore, understanding the con-

trols of weathering can also help to predict the stability of bedrock in rapidly eroding regions.

Reactive transport models are widely used in Earth Sciences to simulate the flow of ground-water through the subsurface (Bethke, 2011). These models can be used to simulate chemical weathering reactions through one-dimensional flow paths based on a few key parameters, which make up the "weathering fingerprint" of a catchment. Models built on different assumptions on weathering control will produce different results. Some of these models are built on a strong temperature control on weathering ("Fontorbe models" from now on, after Fontorbe et al., 2013). More recent models have proposed silicate weathering is more sensitive to runoff than to temperature (Maher, 2011). These ("Maher models" from now on, after Maher, 2011) assume that all weathering paths approach equilibrium. This study looks at Melamchi, a Himalayan catchment north-east of Kathmandu in Nepal, to act as a case study for Himalayan weathering. A proxy is needed for the comparison of the two models, in order to determine which one most accurately represents the weathering in Melamchi.

Estimation of residence time from the Maher and Fontorbe models using measured spring chemistry in Melamchi will act as the proxy for weathering control. The weathering fingerprints of these catchments contain many unknowns, namely the residence time of the water, flow path direction and length, rate of reaction, and extent to which equilibrium is reached. Spring chemistry is reflective of the weathering processes that occur in the subsurface, and can therefore be used to estimate these fingerprint parameters. Residence time, also called the advective age, is defined by how long a given water packet spends from rain recharge into groundwater to exiting at a spring (McCallum et al, 2015). Understanding residence time in particular is important because the geochemical and biogeochemical reactions that contribute to the solute load during weathering are time-dependent; generally, longer residence times promote greater solute accumulation in the water (Berner, 1978). These geochemical reactions are also controlled by the reaction rate which is thought to vary as equilibrium is approached (White and Brantley, 2003; Maher, 2011). Therefore,

an understanding of residence time will provide insight into how long weathering reactions take place in a given catchment, whether they reach equilibrium, and what this means for the carbon cycle as a whole. Residence time will also reflect the variety of flow routes within a catchment because of physical constraints like Darcy's law, which will help to improve hydrological models. Calculating residence time using the spring chemistry in Melamchi will allow the assumptions underlying the two models to be tested, and assess their applicability to a real-world catchment.

From the model comparison will also come a better understanding of fluid residence times in Himalayan catchments, for which tracer data is already commonly used to infer how long a water packet spends in the subsurface (Atwood et al, 2021). Previous studies on Melamchi have used CFC and SF₆ gases to determine a mean age on the order of ten years for groundwater at the base of the catchment ridge (Atwood et al, 2021) (ref map). Using the chemical composition of the water will provide a different way of obtaining residence times, and give a benchmark for the tracer data, which is often reported to be limited in its application (McCallum et al, 2015). If the residence time of a particular water packet is long enough, the reaction will reach chemical equilibrium, meaning the free energy of the system will be close to zero (Kampman et al., 2013). Comparison of these residence times with separate estimates of free energy derived from the measured concentration of springwater in the catchment will test the validity of the two models and their assumptions. Finally, this will help to inform whether weathering in catchments like Melamchi is most strongly controlled by temperature or runoff.

Rates of reaction during weathering comprise both dissolution and precipitation, and chemical equilibrium is defined as that state where these are balanced and equal. The rate of weathering is dependent on the mineralogy of the rock. Different minerals weather at different rates. The most reactive minerals will disproportionately contribute to the solute load of the water (Shand et al, 1999). Therefore, understanding the primary mineral reaction to model is key when quantifying weathering in a catchment. Rates of reaction are thought to be different depending on whether they are measured in the field or in a

laboratory (Maher et al., 2009). This difference has been explained by denoting 'extrinsic' qualities that are variable in the field, such as permeability, mineral/fluid ratios and different surface areas available to react (White and Brantley, 2003). The rate of reaction of a system has also been linked to the free energy of the system, with laboratory rates being calculated significantly further away from equilibrium than field rates (Kampman et al, 2009). This implies that field localities are closer to equilibrium than laboratory-derived rates might suggest.

Differences in lithology are also thought to affect weathering. Geological differences lead to differences in soil composition, landscape features, vegetation, and climate which in turn affect the rates of reaction. Logically, the contribution of one lithology to weathering is at least in part correlated to its spatial extent in the catchment (Stallard and Edmond, 1983). In the Melamchi catchment, only weathering through carbonic acid is considered. Weathering through sulfuric acid also significantly contributes to the global weathering budget, but its impact is not considered in this study because the marine deposits required for its formation are not present in the Melamchi region (Bufe et al., 2021)

Estimation of porosity is essential for understanding the extent of weathering in a catchment. Understanding how open a rock is to water flow and reaction can constrain the reactive transport models used to estimate residence time. Porosities vary widely across a catchment depending on the rock type encountered (Singh et al, 1987; David et al, 1994). Porosity also increases as a rock becomes more weathered (Marques et al, 2009). Note that in the following models, the porosity value is taken to be an average over a given depth in the subsurface. In Earth Sciences, models of fluid flow – whether in the subsurface or deep within the Earth – are typically categorized based on whether the flow occurs through a porous medium or within large open channels (Pedrazas et al, 2021; Maher, 2011; Kelemen et al, 1999; Jackson et al., 2018). This remains an open debate beyond the scope of this study (though note that in later sections flow paths are depicted as "channels" to facilitate the explanation of reactive transport). Hence, the porosity value used for residence time calculation in the reactive transport models is assumed to be an average. This allows for

both types of flow to be plausible, whether in a highly porous medium or large channels surrounded by less porous rock.

The Indian Summer Monsoon (ISM) in Nepal is characterised by a strong seasonal reversal of winds, which brings heavy rainfall to the region during the summer months, and dry conditions during the winter (Bookhagen and Burbank, 2010). The monsoon brings a large amount of precipitation to the region. Oxygen isotope measurements suggest most of the precipitation occurs in the higher elevation parts of the catchment, and this is supported by remotely sensed rainfall estimates in the region (Acharya et al, 2020; Bookhagen and Burbank, 2010). Precipitation and discharge relationships in the Himalayas have been used to suggest that there is a three month lag in the response of the river to precipitation (Andermann et al., 2012). The residence time of groundwater can be used to quantify this delay and nature of its origin, given that rain is the main source of recharge to the groundwater system (Illien et al, 2021). Seasonal variation in rainfall is thought to relate to different hydrological regimes, whereby river discharge and precipitation are 'coupled' when there is a significant enough amount of water to recharge the groundwater system. (Illien et al, 2021) The seasonal variation in precipitation therefore also translates to a variation in runoff, whereby this is twelve times stronger during the monsoon than during the dry season (Sharma, 1997).

Changes in climate contribute to changes in the monsoonal system dynamics. The start of the monsoon has not changed in Nepal, but the end has been delayed. This has led to more intense precipitation on a per day basis, which is detrimental for crops in the winter season due to lack of moisture. Intense precipitation is also considered the main climatic cause of flooding (Panahi et al, 2015; Baniya et al, 2012). "One-off" landslide events transport as much as four times the flux of sediment deposited in the valley in a year (Chen C et al., 2023). These events are thought to be increasing in frequency over recent years as a result of climate change, increasing the erosion rate in these areas (Adhikari et al, 2023). In particular, effects of a flash flood in 2021 are still visible in the area, with damage done to several bridges and hundreds of families.

In this study, spring and rain samples from the Melamchi region of Nepal are used as a case study to investigate the weathering rates in a kinetically-limited catchment. (ref map) The sample dataset consists of 372 samples spanning four field campaigns over three years (2021-2024), as well as more recent year-long bi-weekly timeseries data from stream and spring samples in sites across the catchment. Of those, 68 were collected in September 2024 by a team with researchers from the University of Cambridge and Kathmandu University for this study. This dataset comprises major ion concentrations, alkalinity, and radiogenic strontium isotopes from the Melamchi catchment.

2 Study Area

The Melamchi-Indrawati catchment (85.441 - 85.601 E, 27.822 - 28.157 N) study area ranges from 790 to 5700 m a.s.l. (metres above sea level). The Melamchi River is a tributary of the larger Indrawati River and runs through the catchment draining an area of 325km².

2.1 Geology and Geomorphic Setting

The geology of Melamchi is characterised by the characteristic banded gneiss, feldspathic schist and laminated quartzite of the Higher Himalayan Crystalline Sequence (HHCS). To the south of the confluence of the Melamchi River to its parent Indrawati river lies the Main Central Thrust (MCT) which separates the HHCS from the Lower Himalayan Sequence (LHS) (Dhital et al, Graf et al). The overall geology is therefore largely comprised of silicate metamorphic rock.

2.2 Climate

Annual mean temperatures in the Melamchi Khola Catchment range from 24°C at base elevation to 8°C at highest elevation sampled (3200 m a.s.l.). The area is characterised by a high erosion rate. The southern Himalayas are characterised by a large topographic gradient. This corresponds to a large temperature gradient contributing to tropical and alpine climates close to one another (Kattel et al, 2012). The westerly winds typical of this latitude are responsible for the dry season in the Himalayas (Bookhagen and Burbank, 2010). The source of precipitation during the Indian Summer Monsoon (ISM) affecting Melamchi is the Bay of Bengal, due to the strong pressure gradient that changes the westerly winds to southerly winds. This temperature gradient reverses in the winter, when the oceans are warm and the High Himalaya is cold. The Melamchi Khola catchment receives over 80% of its rainfall during the monsoon.

Recorded temperatures at the end of the spring flow paths vary with the season, being coldest in November. All seasons show a temperature decrease with increasing elevation,

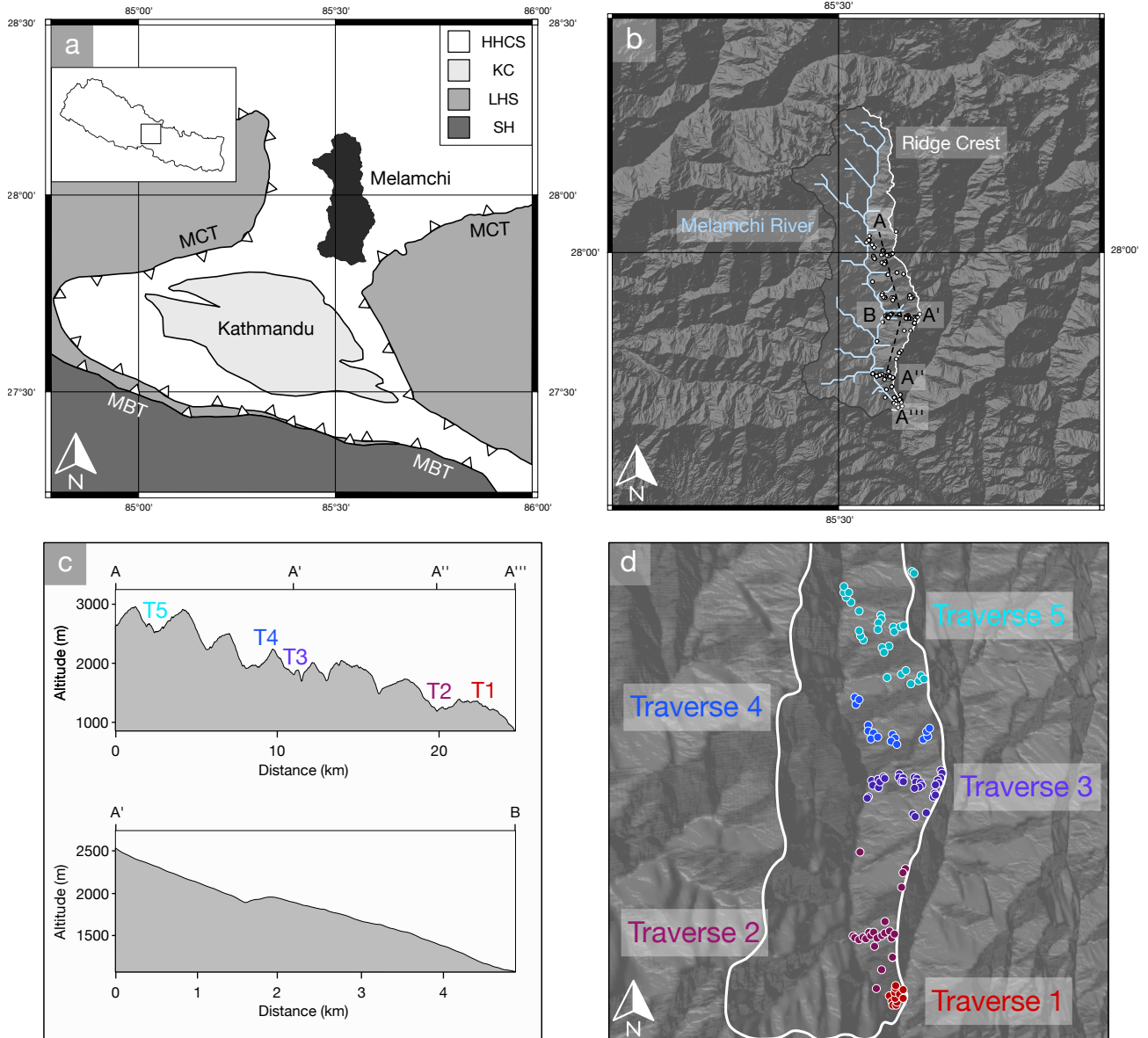


Figure 1: Map of the Melamchi Catchment. a,b,c,d

consistent with the free-air moist adiabatic lapse rate, which is = 6.5 °C/km (Barry and Chorley, 2009). This differs from the annual mean lapse rate in the southern Himalayas of = 5.2 °C/km (Kattel et al., 2013). This disparity could be due to the fact that temperatures may be warmer than air temperatures because of radiative heating. The difference may also be due to systematic errors in temperature measurements; between collection and sampling, warming of the water is plausible.

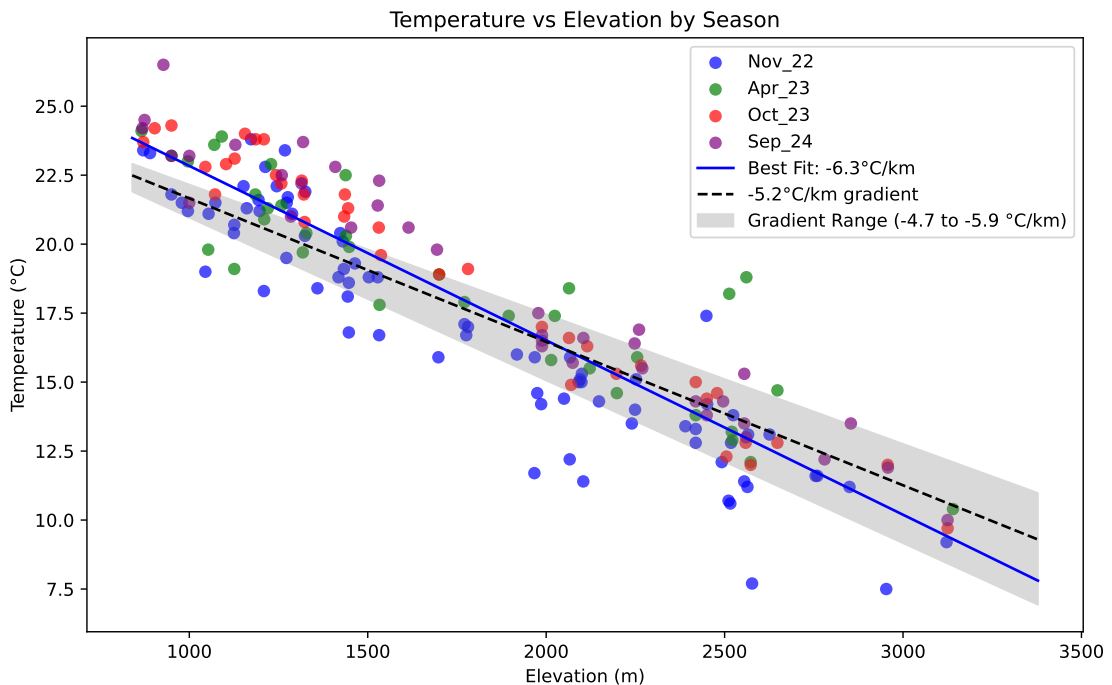


Figure 2: Temperature changes

Catchment	Area	Mean	Mean Ele-	Elevation	Geology	Location	Range
		Slope	vation	Range		(DD)	
		(km ²)	(%)	(m)	(m)		
Melamchi Khola	325	20	2400	786–5697	HHCS	85.441–85.601 E 27.822–28.157 N	

Table 1: Catchment characteristics of the study area.

3 Data Collection and Measurement

3.1 Field Sampling

Both springs and rain were sampled in the field. Springs were sampled according to locations visited in past expeditions. Rain was collected in a rain gauge along several transects. Both water bodies were measured in the field for temperature, pH and TDS on a Hanna Instruments HI-991300 and EXTECH DO700. Samples were also titrated using a Hach digital titrator with 0.0625M HCl to calculate the alkalinity of the water following the Gran Method (Gran, 1952). The field measurements were done 24 hours within having been collected. Six aliquots were collected for each spring for anion, cation, titration, DIC, isotope and archive purposes respectively. Rain samples had a smaller yield and so only three aliquots were collected, for ion, isotope and archive purposes. Both water body types were filtered through a $0.2\mu\text{m}$ PES membrane in a filtration unit prior to bottling. Cation and archive samples were acidified with concentrated HNO_3 to give a pH of ~ 2 , keeping the cations in solution.

3.2 Major and Trace Element Analysis

Cation concentrations were determined using a Agilent Technologies 5100 Inductively-Coupled Plasma Optical Emission Spectrometer (ICP-OES) using a calibration line made from a Nepalese spring stock solution. Anion concentrations were determined using a Dionex Ion Chromatography System (ICS) 5000 series against the Battle-02 standard calibration line. Associated uncertainties range between 5-10% for cations and anions.

4 Methods and Models for Analysis

4.1 Rain and Hydrothermal Correction

Rain input is a significant factor in the chemical composition of groundwater and rivers. Most chloride found in these water bodies is thought to be due to rainwater input (Drever,

1997). It is standard practice to correct for this rain input. Once the samples have been corrected for rain input, the remaining chloride is assumed to be derived from hydrothermal signatures encountered in the flow path. Spring waters are also therefore corrected for hydrothermal input, so that the concentrations used for modelling are strictly derived from weathering reactions.

4.2 Identifying the Weathering Reaction

The first step towards quantifying the extent to which chemical weathering reactions have gone to completion is to discern what reaction is taking place. In principle this is as simple as knowing what minerals are dissolving and which are precipitating. Modal decomposition methods consider several minerals that could be dissolving and/or precipitating, and their stoichiometry (Garrels and Mackenzie, 1967; Drever, 1997). Note that this calculation can only be done if the number of components is the same as or greater than the number of minerals.

$$\begin{array}{ccccccc}
 & Biot & Plag & Calc & Smec & Kaol & K Spar & Spring(\mu\text{mol/l}) \\
 Si & a_{11} & a_{12} & a_{13} & a_{14} & a_{15} & a_{16} & b_1 \\
 Al & a_{21} & a_{22} & a_{23} & a_{24} & a_{25} & a_{26} & b_2 \\
 Mg & a_{31} & a_{32} & a_{33} & a_{34} & a_{35} & a_{36} & b_3 \\
 Ca & a_{41} & a_{42} & a_{43} & a_{44} & a_{45} & a_{46} & b_4 \\
 Na & a_{51} & a_{52} & a_{53} & a_{54} & a_{55} & a_{56} & b_5 \\
 K & a_{61} & a_{62} & a_{63} & a_{64} & a_{65} & a_{66} & b_6
 \end{array} \cdot \begin{pmatrix} x_{Biot} \\ x_{Plag} \\ x_{Calc} \\ x_{Smec} \\ x_{Kaol} \\ x_{K Spar} \end{pmatrix} = \begin{pmatrix} b_1 \\ b_2 \\ b_3 \\ b_4 \\ b_5 \\ b_6 \end{pmatrix}$$

Matrix algebra facilitates the calculations of the mineral proportions in the water. Given known matrices A and B , where A represents the stoichiometric quantities of elements in a mineral, and B the concentrations of elements in the water:

$$AX = B \quad (1)$$

$$X = A^{-1}B \quad (2)$$

The matrix X, corresponding to volumetric proportions of the minerals in the water, can then be calculated, under the assumptions that all minerals dissolve in a congruent fashion. Modal decomposition for spring waters was performed according to stoichiometric proportions from Bickle et al. (2015). For ease of visualisation, Figure 3 shows the positive, dissolved minerals on the LHS, and the negative, precipitated minerals on the RHS.

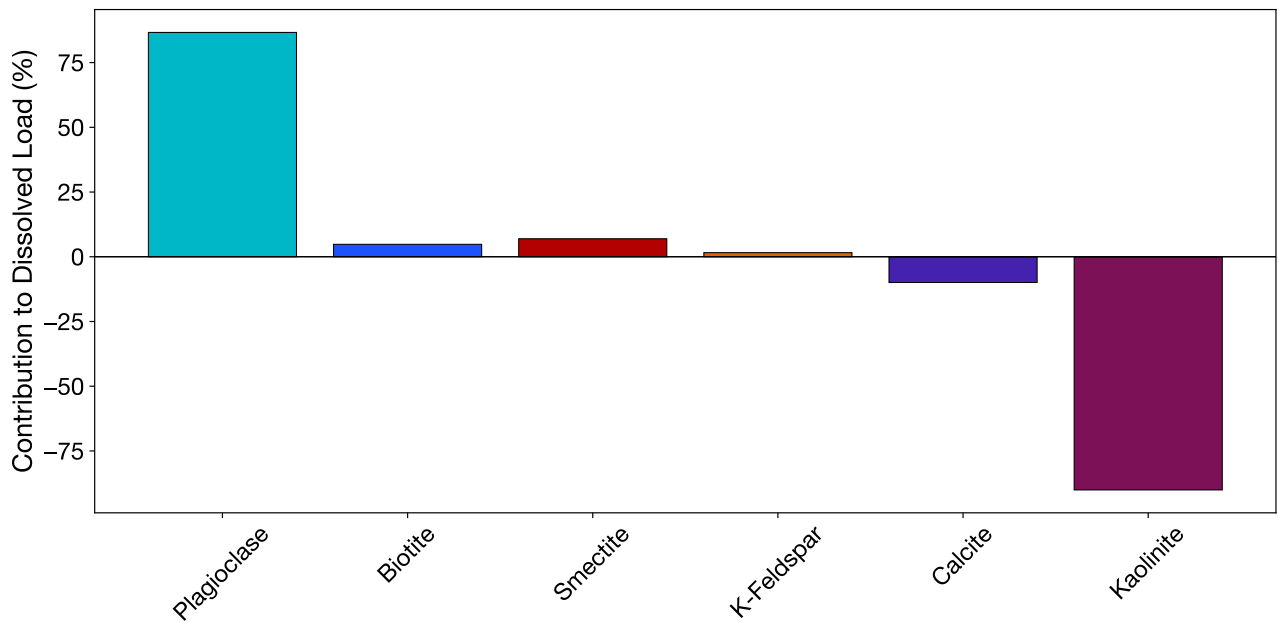
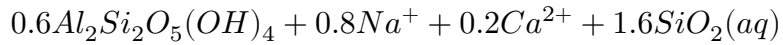
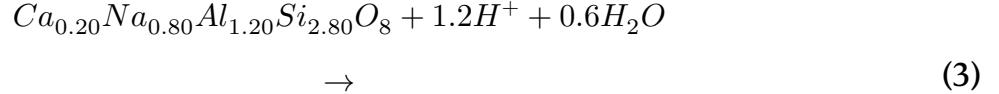
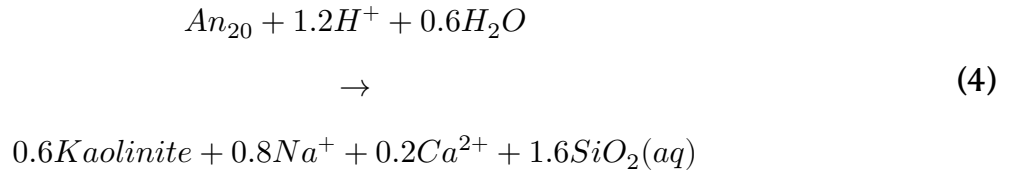


Figure 3: Average of the modal decomposition for all springs.

Figure 3 is representative of most springs in Traverse 3. Hence, the major phase being dissolved is plagioclase feldspar and the major phase being precipitated is kaolinite. The primary composition of plagioclase in the area corresponds to \approx An-20 (Bickle et al., 2015; Knight et al., 2024). The plagioclase to kaolinite reaction is given by the following equation (written so that aluminium is conserved):



Or

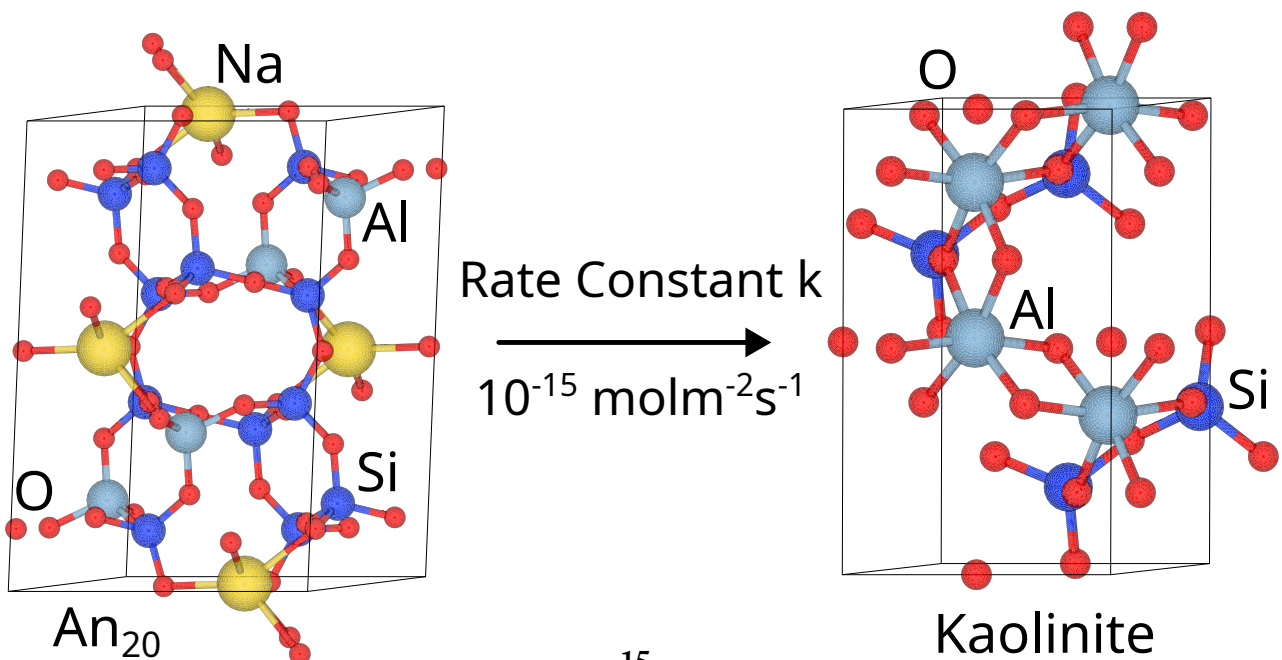
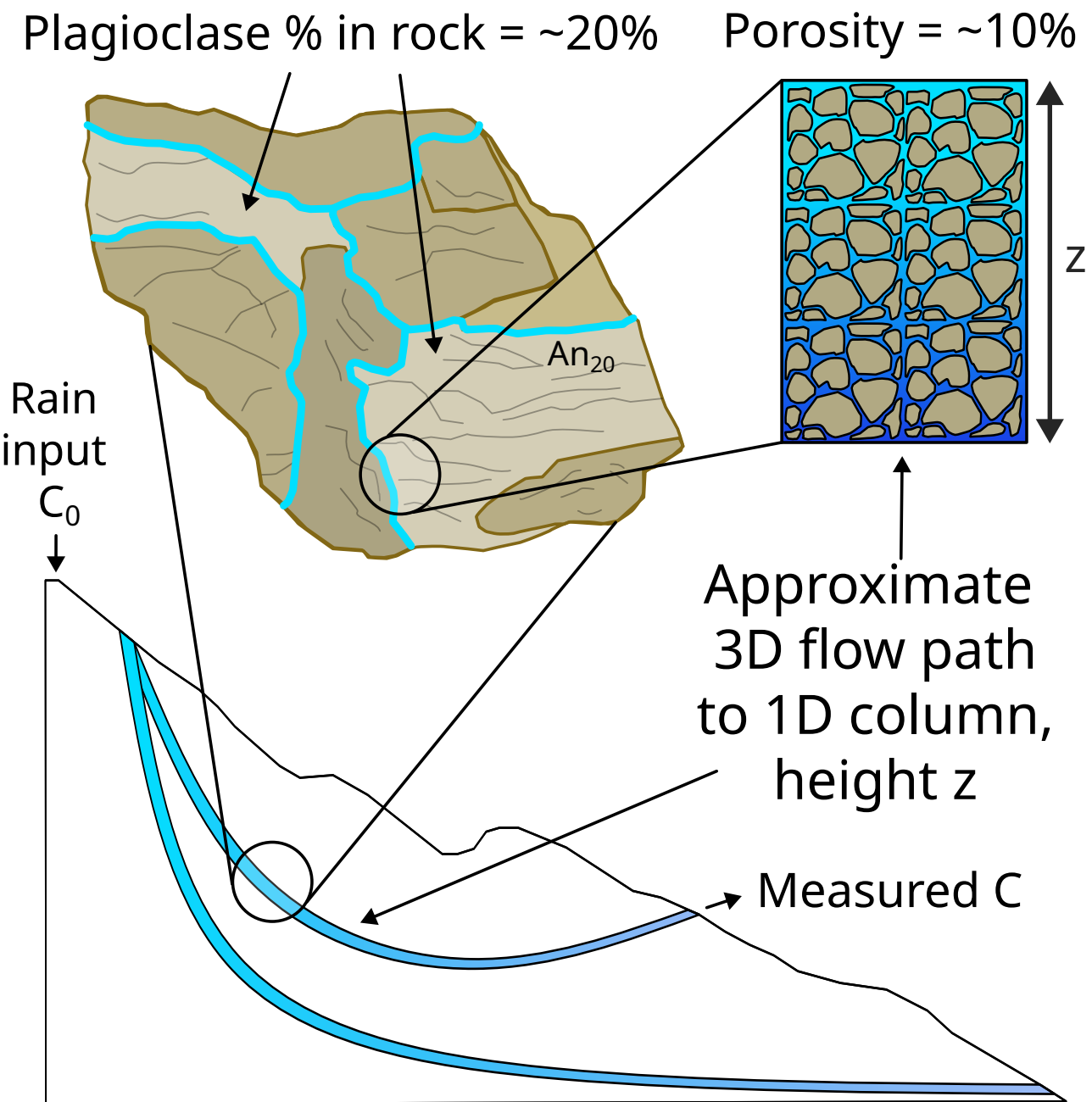


4.3 One-Dimensional Reactive Transport Models

Reactive transport models are widely used in applied fluid dynamics and various fields within Earth Sciences. These models aim to track chemical reactions occurring at each spatial point, accounting for the movement of reactants to and reaction products away from those points (Bethke, 2011). The basic form of a reactive transport model is a partial differential equation that describes the transport of solutes and the reactions that occur between them. For reacting solutes, concentration changes over time are governed by transport rates – derived from the divergence principle – and the relative rates of dissolution and precipitation (Bethke, 2011). These models simplify a real world three-dimensional catchment into one-dimensional flow paths. Additionally, as described in the Introduction ref, porosity is chosen to be a representative average over the whole subsurface; this allows for the results to feasibly represent residence times that come from channelised or slow porous flow. The proposed equations can be complex, but in simple cases a species of concentration C_i can be modelled to follow a first-order rate law, generally represented by:

$$\frac{\partial C_i}{\partial t} = \mathcal{O}_T(C_i) + \mathcal{O}_R(C_i) \tag{5}$$

Where \mathcal{O}_T and \mathcal{O}_R are the transport and reaction operators, respectively (Bethke, 2011). Depending on the hypothesis supported, equation 5 can be modified accordingly. The following sections will discuss two models with their own versions of equation 5.



Model Motivation

As discussed in the Introduction (ref), there are different hypotheses regarding the major controls on chemical weathering. This section will contrast one model following the hypothesis that weathering is most sensitive to temperature (Fontorbe et al., 2013), and another model that suggests weathering is more sensitive to the hydrological cycle (Maher, 2011; Maher and Chamberlain, 2014). The benchmark for a model's effectiveness will be how well it can predict residence times compared to previous studies on gas tracers. Assumptions and constraints will be compared and contrasted, and their results used to inform the calculation of rates of reaction and approach to equilibrium in Melamchi. For both models, the element used to benchmark is dissolved silicon. This is because silicon is present in both dissolution and precipitation reactions, so it is applicable to the Maher model which considers both reactions. Furthermore, silicon is what both models were used for in their respective original studies.

Fontorbe et al. (2013) - Model

This model investigates silicon isotopic composition in the Ganges River, assuming constant reaction rates along flow paths (see Appendix for a full derivation, and Table ref for a list of parameters used). This model was initially constructed to reproduce DSi concentration and $\delta^{30}\text{Si}$ in the Ganges, but is being repurposed in a novel fashion for this study. The first-order differential equation governing transport and reaction is given as:

$$\phi \frac{\partial C}{\partial t} = -\omega \phi \frac{\partial C}{\partial z} + R_n(1 - f) \quad (6)$$

Where C is the elemental concentration, ω is the fluid velocity, ϕ is the rock porosity, z is a position along the flow path, R_n is the rate of reaction, and f is the fraction of Si present in the dissolved load that is reprecipitated in the back reaction. The equation can be nondimensionalised using the Damköhler number (N_D), which describes the relative importance

of kinetic vs transport-controlled settings (Bethke, 2008):

$$N_D = \frac{R_n h}{\phi C_0 \omega} \quad (7)$$

Assuming steady-state ($\partial C / \partial t = 0$), the concentration at the end of the flow path can be rearranged to give the residence time T_f :

$$T_f = \frac{(C - C_0)\phi}{(1 - f)R_n} \quad (8)$$

Fontorbe			
Parameter	Definition	Units	Formula (Value)
ϕ	Porosity	-	0.1*
ω	Fluid velocity	m/s	Variable
h	Length of flow path	m	Variable
C	Concentration end of flow path	$\mu\text{mol/L}$	Variable
C_0	Initial concentration	$\mu\text{mol/L}$	Rain Input
f	Fraction reprecipitated	-	0.5*
N_D	Damkohler Number	-	$N_D = \frac{R_n h}{\phi C_0 \omega}$
T_f	Residence time	s	$T_f = \frac{h}{\omega \phi}$
R_n	Reaction rate	$\text{mol}/\text{m}^3/\text{s}$	$\rho \cdot 10^6 \cdot k \cdot S \cdot X$
k	Reaction rate constant	$\text{mol}/\text{m}^2/\text{s}$	10^{-15*}
S	Specific surface area	m^2/g	0.1*
ρ	Plagioclase density	g/cm^3	2.7*
X	Volume fraction of mineral in rock	g_{min}/g_{rock}	0.2*

Table 2: Key parameters and definitions for the Fontorbe model. Starred terms are values used for calculation.

Maher and Chamberlain (2014) Model

This model is built in accordance with the principle that the main control on silicate weathering is hydrological cycle, namely how much water passes flows a particular path. The model is based on the assumption that the reaction rate decreases linearly with approach to equilibrium, and that all weathering paths approach equilibrium. The motivation behind the hydrological control is based on sensitivity analyses of real catchment data on one-dimensional reactive transport models which suggest that porosity, mineral surface area, and temperature have no consistent correlation with water composition (Maher, 2011). See Appendix and Table ref for a full derivation and the model parameters respectively. The model begins with the following representation of the concentration of a solute in a fluid flow path:

$$\frac{dC}{dt} = -\frac{q}{\theta} \frac{dC}{dz} + \sum_i \mu_i R_{d,i} \left(1 - \left(\frac{C}{C_{eq}}\right)^{n_i}\right)^{m_i} - \sum_i \mu_i R_{p,i} \left(1 - \left(\frac{C}{C_{eq}}\right)^{n_i}\right)^{m_i} \quad (9)$$

Where C is the concentration, q is the fluid flux, θ is the volumetric water content, z is the position along the flow path, μ is the stoichiometric coefficient, R is the rate of reaction for dissolution and precipitation respectively, C_{eq} is the equilibrium concentration, and n and m are non-linear parameters (Maher and Chamberlain, 2013). For a given packet of water, R_n is defined as:

$$R_n = R_d - R_p \quad (10)$$

$$\frac{dc}{dt} = R_n \left(1 - \frac{C}{C_{eq}}\right) \quad (11)$$

Where R_d and R_p are the rates of dissolution and precipitation respectively. This can be solved for concentration, and rearranged for residence time to obtain:

$$T_f = \frac{C_{eq} \cdot (C - C_0)}{e^2 R_n (C_{eq} - C)} \quad (12)$$

Note the e^2 term is used because the Maher model considers all paths as if they approach equilibrium.

Maher			
Parameter	Definition	Units	Formula (Value)
ϕ	Porosity	-	0.1*
h	Length of flow path	m	Variable
q	Flow rate	m/s	Variable
C_{eq}	Equilibrium concentration	$\mu\text{mol/L}$	Max Catchment
C_0	Initial concentration	$\mu\text{mol/L}$	Rain Input
R_n	Net reaction rate	mol/L/s	$\rho \cdot 10^6 \cdot k \cdot S \cdot X$
ρ	Plagioclase density	g/cm^3	2.7*
k	Reaction rate constant	$\text{mol/m}^2/\text{s}$	10^{-15*}
S	Specific surface area	m^2/g	0.1*
X	Volume fraction of mineral in rock	g_{min}/g_{rock}	0.2*
τ	Scaling factor	-	$\tau = e^2$
D_w	Damkohler Coefficient	m^2/s	$D_w = \frac{L\phi R_n}{C_{eq}}$
T_f	Residence time	s	$T_f = \frac{h\phi}{q}$

Table 3: Key parameters and definitions for the Maher model. Starred terms are values used for calculation.

4.4 Estimates of Uncertainty

Uncertainties were propagated using a Monte Carlo method using an assumed normal distribution. Both the observed parameters and estimated parameters have uncertainties associated to them.

Parameter Definitions and Propagated Uncertainties				
Parameter	Definition	Units	Value	Uncertainty
ϕ	Porosity	-	0.1	$\pm 10\%$
C_{eq}	Equilibrium DSi concentration	$\mu\text{mol/L}$	$869 \mu\text{mol/L}$	$\pm 10\%$
C_0	Initial DSi concentration	$\mu\text{mol/L}$	$95 \mu\text{mol/L}$	$\pm 10\%$
ρ	Plagioclase density	g/cm^3	2.7	$\pm 10\%$
k	Reaction rate constant	$\text{mol/m}^2/\text{s}$	10^{-15}	$\pm 10\%$
S	Specific surface area	m^2/g	0.1	$\pm 10\%$
X	Volume fraction of mineral in rock	$\text{g}_{\text{min}}/\text{g}_{\text{rock}}$	0.2	$\pm 10\%$
f	Fraction reprecipitated	-	0.5	$\pm 10\%$
ΔG^0	Standard Gibbs Free Energy	kJ/mol	$-\text{RTlnK}^*$	$\pm 10\%$

Table 4: Key parameters, definitions, and propagated uncertainties. * Uncertainty associated with temperature and K calculated from pgcc using The Geochemist's Workbench® Rxn program(ref)

5 Results: Spring Chemistry and Residence Time

5.1 Traverse 1

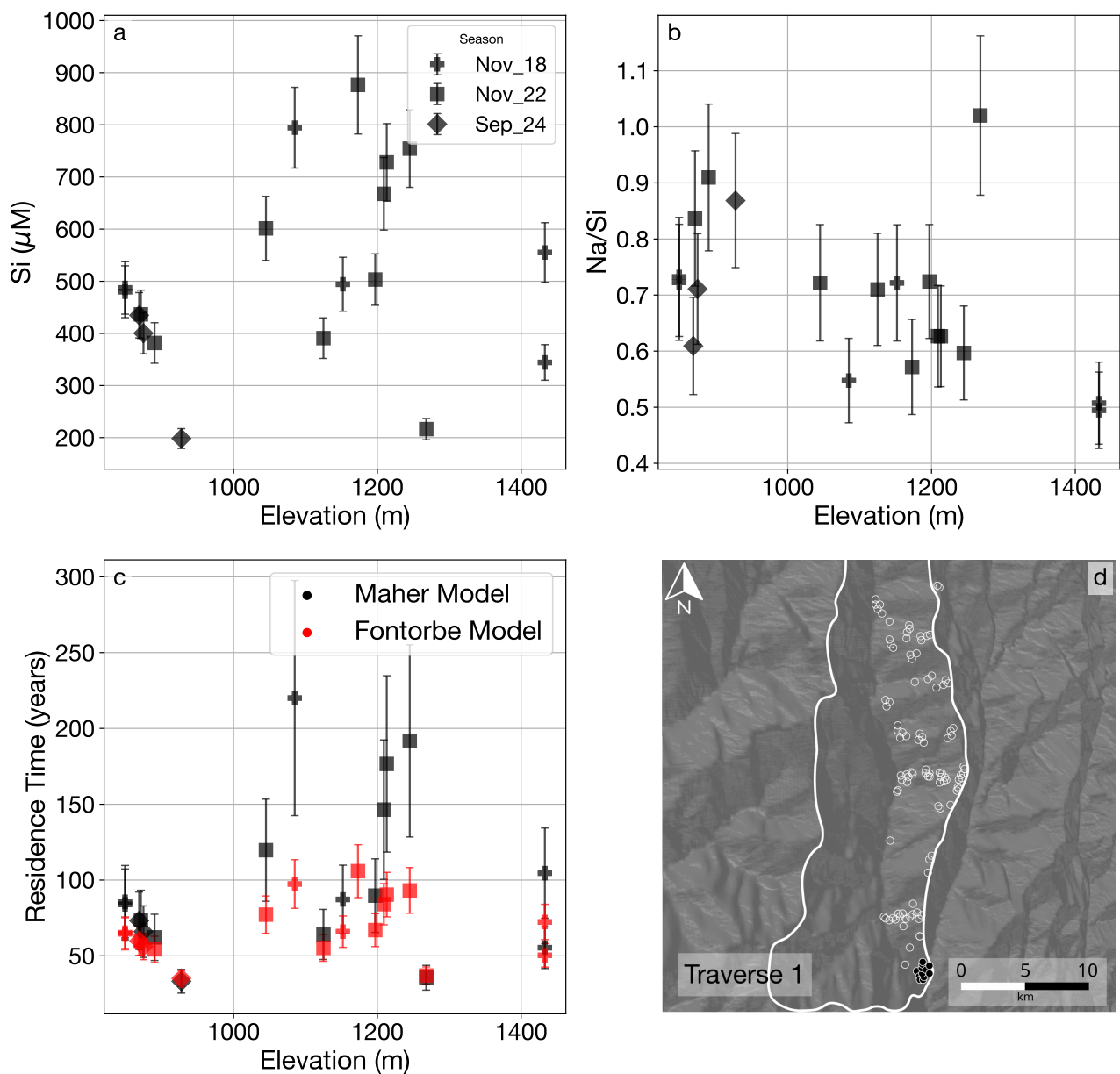


Figure 5: Traverse 1 - Variations in Spatial Chemistry

Concentration of dissolved silicon (DSi) in the springs sampled in Traverse 1 is at a maximum for the whole catchment. There is no clear trend of increasing DSi concentration or Na/Si with decreasing elevation. The Fontorbe model predicts a peak of ≈ 100 years, while the Maher model predicts a much higher residence time of ≈ 600 years.

5.2 Traverse 2

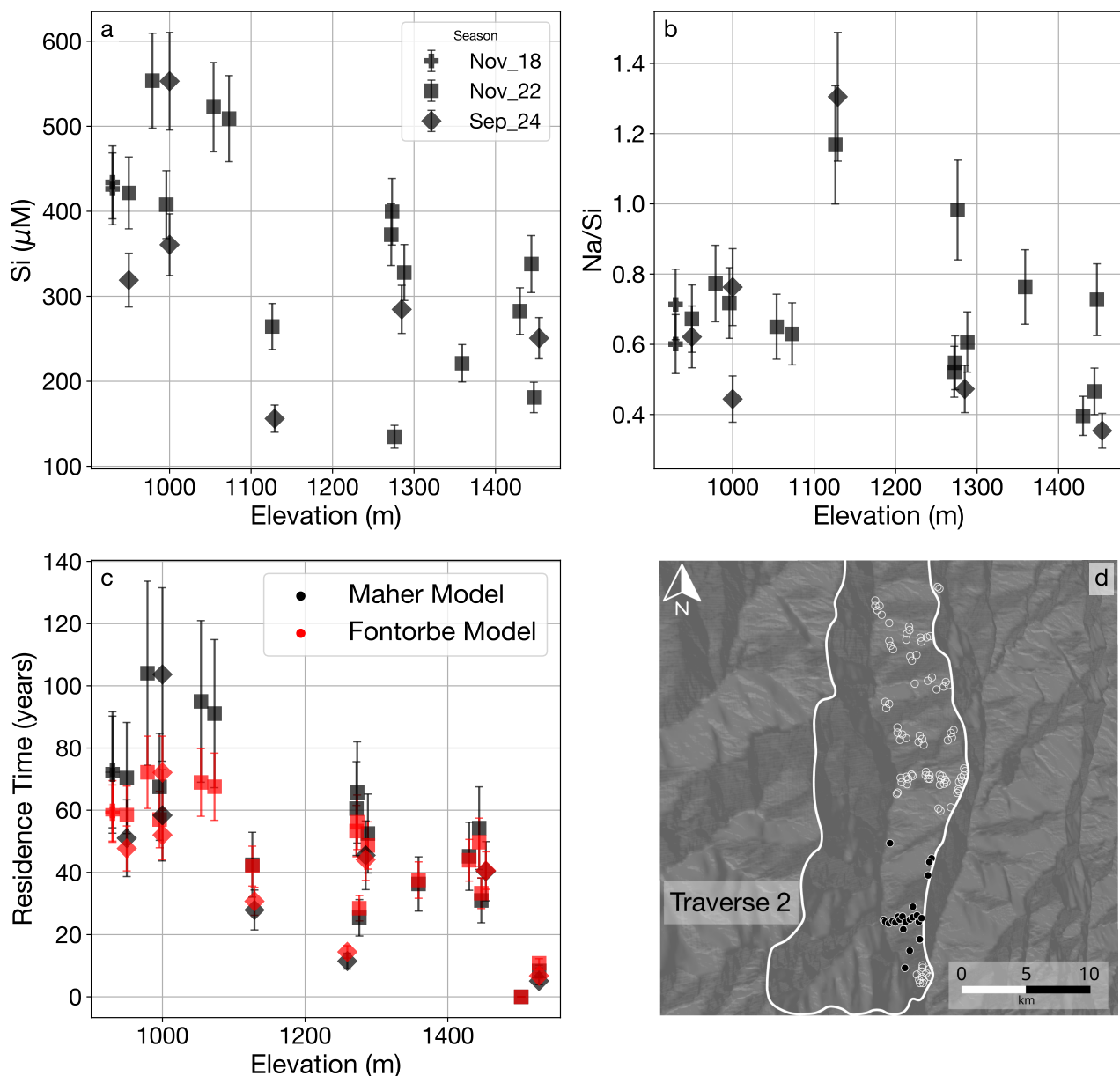


Figure 6: Traverse 2 - Variations in Spatial Chemistry

Dissolved silicon concentration shows a clear increase in concentration with decreasing elevation. There is no resolvable trend with Na/Si and elevation, nor with different seasons when it was collected. Residence times are generally lower than those in Traverse 1. The Fontorbe model predicts generally older times than the Maher model at higher elevations, and younger times at lower elevations.

5.3 Traverse 3

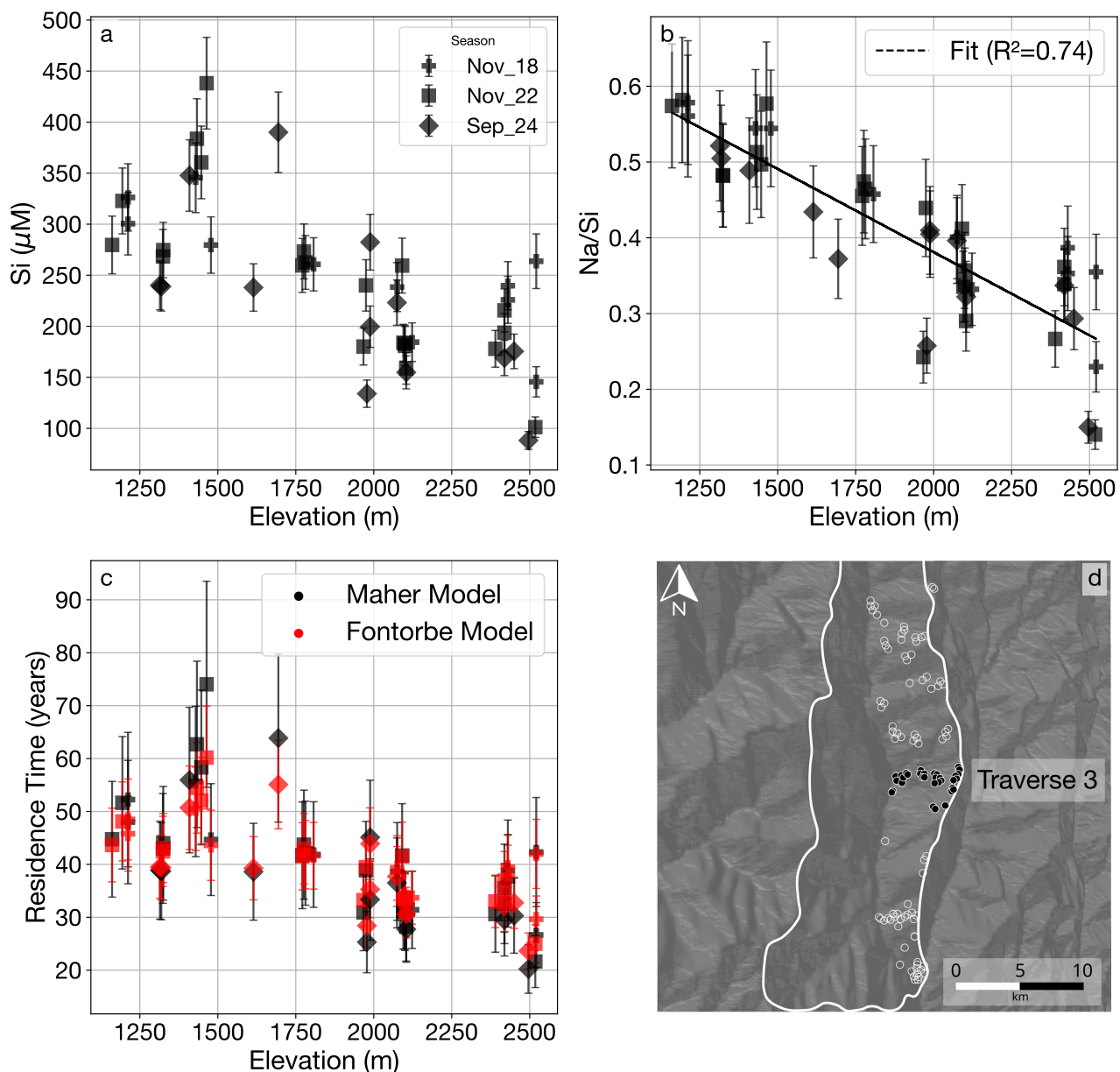


Figure 7: Traverse 3 - Variations in Spatial Chemistry

Dissolved silicon concentration increases with decreasing elevation in Traverse 3. There is a potential dip at the lowermost elevation sampled. Na/Si increases with decreasing elevation, consistent between different sampling seasons. Estimated residence times increase as elevation decreases, peaking at ≈ 50 years for the Maher model. This peak occurs at the same elevation as the highest DSi concentration.

5.4 Traverse 4

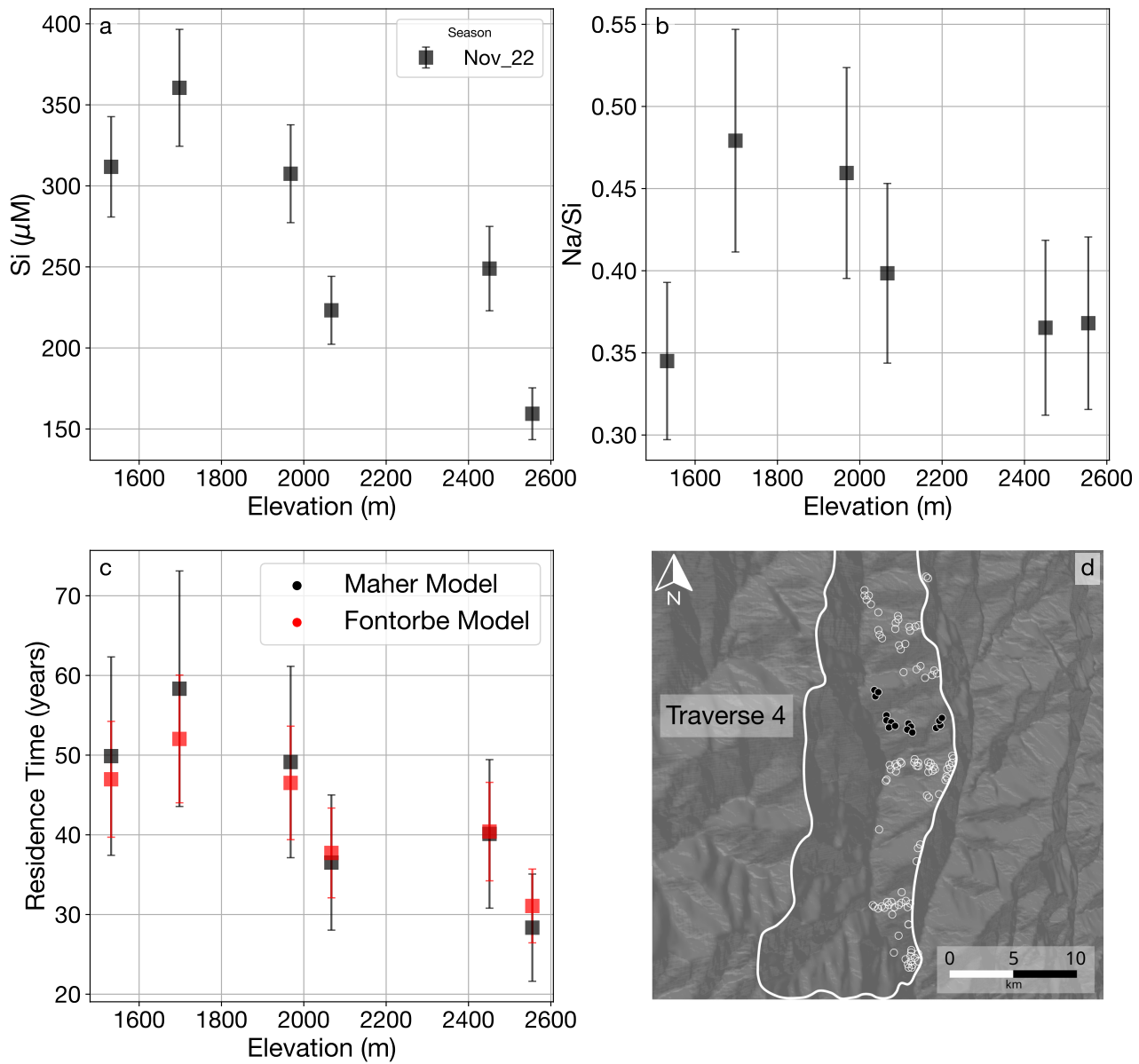


Figure 8: Traverse 4 - Variations in Spatial Chemistry

Traverse 4 is undersampled compared to the other traverses. Given the small sample set, any apparent trend is less likely to be reflective of the true chemistry. Nevertheless, DSi increases with decreasing elevation as seen in some of the previous traverses. There is no discernable trend with Na/Si. Residence times also increase with decreasing elevation, with the Maher model predicting younger times at the highest elevations, and older times at the lowest elevations. The highest residence times predicted are ≈ 35 years.

5.5 Traverse 5

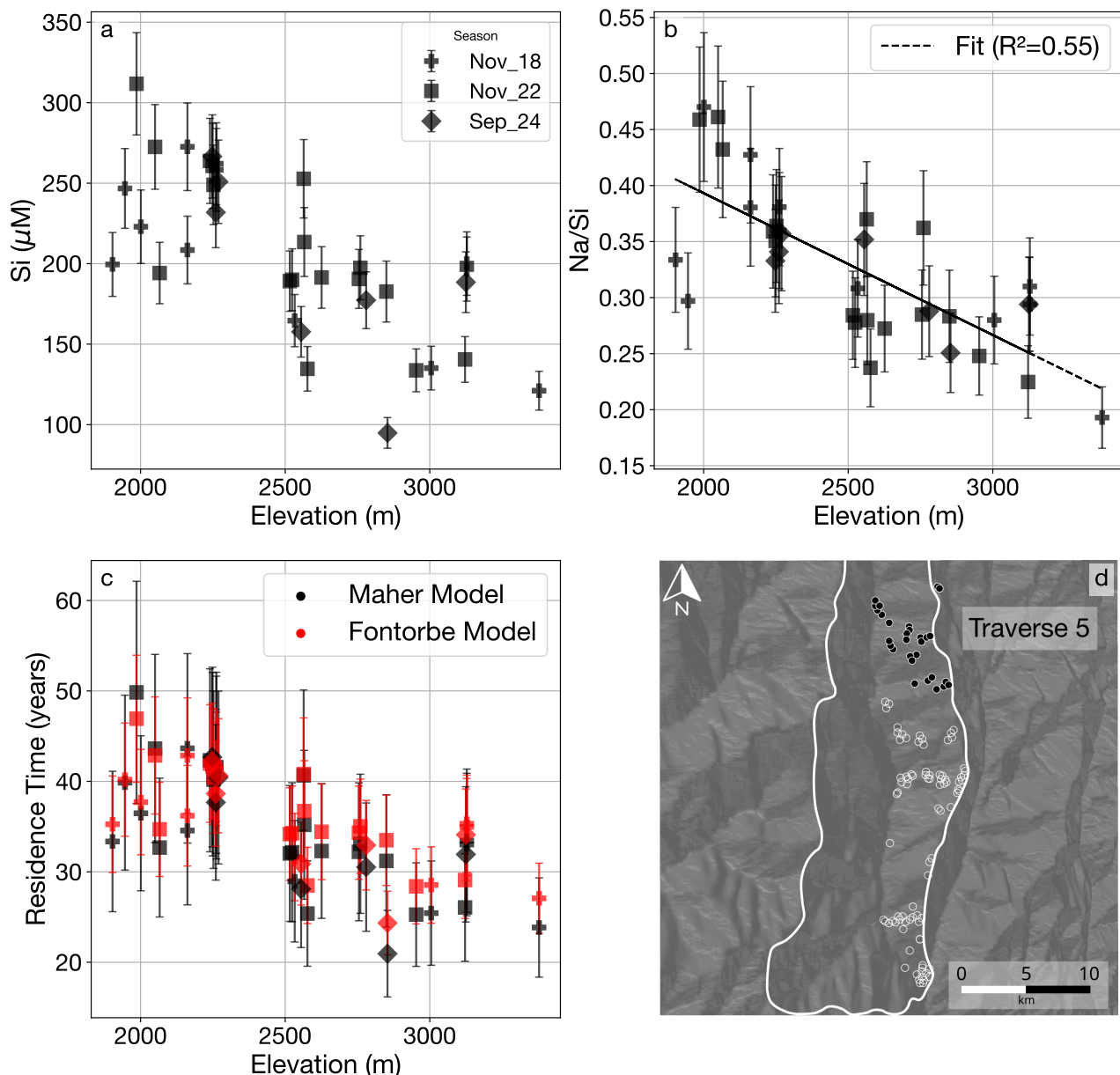


Figure 9: Traverse 5 - Variations in Spatial Chemistry

Traverse 5 is highly sampled and sits at the highest elevation of the whole catchment. DSi concentration increases with decreasing elevation but there is scatter in the data. Na/Si similarly shows a trend of increasing ratio with decreasing elevation, and it is replicated between different seasons, with considerable scatter. Residence times are the lowest predicted in the catchments.

5.6 Time Series Trends

Concentrations of dissolved silicon in several springs in the catchment show a consistent decrease in concentration with the onset of the monsoon. Concentrations are high in April, decrease to a minimum in September, then slowly increase back to April levels through October and November. Decrease in concentration is likely a sign of dilution from increased precipitation during the monsoon. Such a trend is also present in a time series of a spring in Traverse 3. The average April-September decrease is small compared to the average dissolved silicon concentration of the rain.

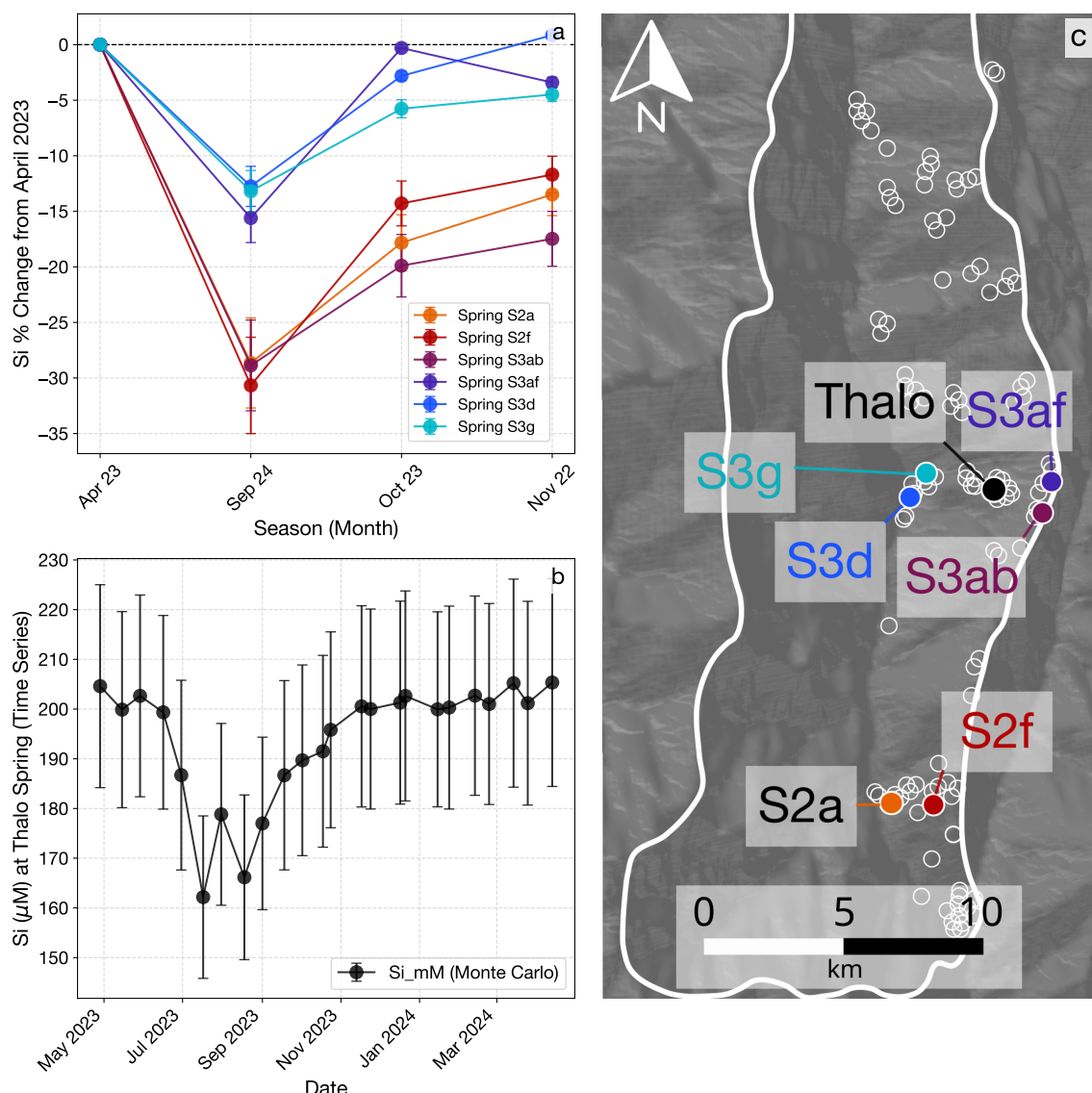


Figure 10: Seasonal changes in spring concentration indicating monsoonal precipitation influence.; Time series of spring concentration changes over time.

6 Discussion

6.1 Explaining Traversal Variations in Chemistry

Increasing DSi concentration with decreasing elevation suggests the springs are sampling increasingly longer flow paths. This is because longer flow paths allow for more water-rock interaction, which scavenges more Si from the silicate rocks. While most traverses show such a trend, this does not happen in Traverse 1. There are several possible reasons for this. For one, the lowermost springs are likely to be close to the Melamchi river which is more dilute than the most concentrated springs in the traverse. Mixing with the river waters is possible but unlikely because of the difference in elevation. It is unlikely that the decrease is caused by a dilution effect at the start of the monsoon such as that shown in Figure (ref). This is because these DSi trends are consistent across multiple seasons within error. Clearly, however, samples collected in September will be relatively more dilute than those collected in April.

A decrease in Si at lower elevations here could also suggest precipitation of secondary minerals. Linear trends in plot (b?) for Traverses 1, 3, and 5 show an increase in Na/Si as elevation decreases. Si is involved in the backward secondary mineral precipitation weathering reaction, and Na is not, as evidenced in equation (?). In other words, elevated Na/Si is interpreted as a sign of a closer approach to equilibrium, as more Si is scavenged from the water to form secondary precipitates, while the Na is only involved in dissolution. This is consistent with the Traverse 1 springs having the highest concentrations of Si in the catchment as chemical equilibrium is approached.

Plots of Na/Si against elevation coloured by season can also be used to infer how consistently a given flow path is sampled. Because Na/Si is primarily controlled by the balance of dissolution and reprecipitation, and by extension the average age of water in the flow path, consistency of this value over time points to the same flow path length being sampled for a given rate of reaction. Under the steady state assumption assumption $\partial C / \partial t = 0$ used

in the residence time models, the Na/Si ratio should be constant over time at a given elevation if the same flow path is sampled. For both Traverse 3 and 5, the Na/Si ratio against elevation does not change between different seasons. However, there is a better correlation in Traverse 3 which suggests the flow paths here are more consistently sampled.

6.2 Residence Time Agreement with Gas Ages

As shown in Figures (? ,? ,? ,?), predicted residence times in the catchment are consistent between the Maher and Fontorbe Models. Residence times increase as elevation decreases, agreeing with the notion that springs sampled at these lower elevations reflect longer flow paths. Residence times in Traverse 3 can be directly compared to the gas ages obtained by Atwood et al. (2021), because both studies are sampling the same springs. The Atwood et al. ages in Traverse 3 range from 5-35 years. The findings from this study and both models predict residence times of a similar order of magnitude. This study does predict slightly longer times at the lowest elevation, but this discrepancy is within the range of propagated uncertainty. Using spring chemistry is therefore a viable method to determine residence times in natural catchments, with the premise that the model assumptions are valid. In addition, this study lends credibility to the use of gas ages to determine residence times, which is an approach that is often criticised for using biased age distributions (McCallum et al., 2015). Findings of residence times on the order of 10-100 years for the whole catchment also inform precipitation-discharge relationships. If this study's findings are correct, then the delay in river discharge found by Andermann et al. (2013) is likely only recording surface or near-surface flow. The shorter flow paths here could plausibly be associated to residence times of a few months.

Because both models agree with Atwood et al. (2021), however, it is difficult to discern which one is more appropriate to use for real world catchments like Melamchi, and so determine what the greatest control on weathering there is. In order to do this, then, the underlying assumptions of the models must be tested.

6.3 Free Energy Calculations suggest Far From Equilibrium System

One of the main assumptions of the Maher model is that all flow paths reach equilibrium. The free energy of reaction, calculated using the activity of the ions in solution, can be used in natural systems to determine the extent to which equilibrium is reached (Kampman et al., 2014; Wojicki, 2011). Free energies lower than -10 kJ/mol are considered close to equilibrium, whilst those more negative than -40 kJ/mol are categorised as far from equilibrium (Kampman et al., 2014). This method can therefore test the validity of the Maher model in Melamchi. Free energy is defined as:

$$\Delta G = \Delta G^0 + RT \ln Q \quad (13)$$

As discussed in (ref methods), the weathering reaction characterising this catchment is the dissolution of plagioclase (An-20) to precipitate kaolinite, given by eq (ref). The exact composition of plagioclase is important for these calculations. The free energy of reaction is lowered by the presence of a solid solution between albite and anorthite (Dubacq, 2022). The parameters for the standard free energy of reaction are calculated using the pygcc python package (cite). The package gives the standard properties of solid-solution species and reactions, such that ΔG^0 can be calculated:

$$\Delta G^0 = \Delta G_{products}^0 - \Delta G_{reactants}^0 = -RT \ln K \quad (14)$$

K is calculated using the database obtained from pygcc using The Geochemist's Workbench® Rxn program(ref). Q is calculated as the ion activity product of the reaction, assuming the activities of the solid phases plagioclase and kaolinite are 1, the activity of water is 1, and the activity of the ions in solution are equal to their concentration.

$$Q = \frac{a_{\text{Kaol}}^{0.6} a_{\text{Na}^+}^{0.8} a_{\text{Ca}^{2+}}^{0.2} a_{\text{SiO}_2(\text{aq})}^{1.6}}{a_{\text{An}_{20}} a_{\text{H}^+}^{1.2}} \quad (15)$$

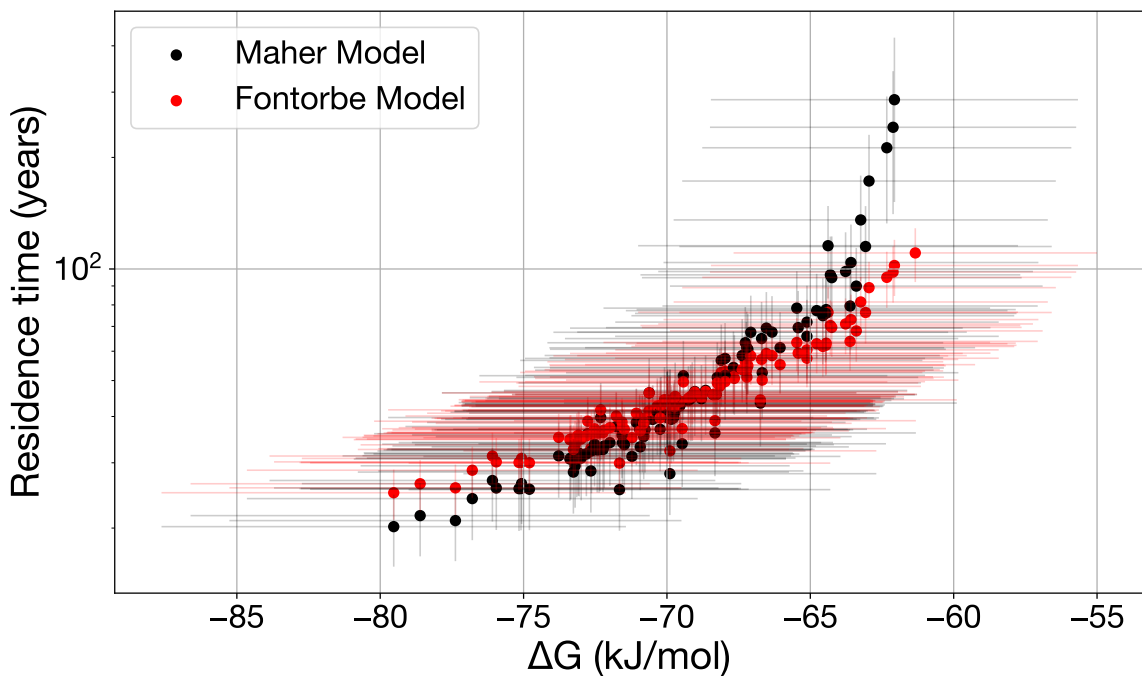


Figure 11: Comparison of the delta G obtained against elevation. Comparison of delta G with residence time for both models

Calculated free energy shown in Figure 11 shows that all springs in the catchment have a free energy that is more negative than -40 kJ/mol. These samples are therefore classified as far from equilibrium. Figure 11 does show that free energy gets closer to zero as residence time increases. This is consistent with the notion that groundwaters approach equilibrium the more they stay in the subsurface and react. However, the extent of reaction is not great enough to be considered close to equilibrium. This suggests that, for Melamchi, using the Maher model to estimate residence times is not appropriate, and so the greatest control on weathering is temperature. This is more apparent when considering the residence times predicted at the southernmost Traverse 1.

6.4 Model Pitfalls

Residence times in Traverse 1 are explainably the longest in the catchment. The springs here are at the lowest elevation, so the flow paths are presumably the longest. This is consistent with the highest DSi concentration of the catchment, and evidence for secondary precipitation of kaolinite at the lowest elevations (See Figure ?b). In Traverse 1, the Fontorbe model predicts a peak of ≈ 100 years, while the Maher model has a much higher residence time of ≈ 600 years. The discrepancy is likely due to how the models are formulated.

Fontorbe	Maher
$T_f = \frac{(C_h - C_o) \cdot \phi}{(1 - f) \cdot R_n}$	$T_f = \frac{C_{eq} \cdot (C - C_0)}{e^2 R_n (C_{eq} - C)}$

Table 5: Comparison of equations from Fontorbe and Maher

The difference in the models comes from the underlying assumptions of reaction rate and how it changes towards equilibrium. Reaction rate is kept constant in the Fontorbe model assuming a far from equilibrium state. In the Maher model, reaction rate depends on the equilibrium concentration. It is unrealistic that reaction rate continue to be constant as the reaction progresses, and so the Maher model more accurately reflects water that is close to equilibrium. Indeed, as equilibrium concentration is reached in the Maher model, the reaction rate will decrease. In order to produce more concentrated springwaters as in Traverse 1, the groundwater must have a longer residence time. The $\frac{C_{eq}}{(C_{eq} - C)}$ term in the Maher model gets larger as the concentration approaches equilibrium. As a result of this, the Maher model consistently predicts longer residence times than the Fontorbe Model at higher DSi concentrations, while the opposite is true at lower DSi concentrations. It also follows that for Traverse 1 the $\frac{C_{eq}}{(C_{eq} - C)}$ term grows arbitrarily large, hence the strong discrepancy found in Figure (?c).

For this study's calculations, the equilibrium concentration is taken to be the highest in the catchment, $869 \mu\text{M DSi}$. This concentration corresponds to the highest spring concentration found in Traverse 1. Note that in the Maher and Chamberlain (2014) model setup, an equilibrium concentration of $375 \mu\text{M DSi}$ is chosen from the global river data of Gaillardet et al. (1999). This is sound for a theoretical model but is not appropriate for this catchment. It is unclear, however, whether choosing the highest DSi concentration in the catchment is appropriate. Clearly as this concentration is approached, the Maher model will predict unrealistic residence times, as shown in Figure 11. The free energy of the system suggests the spring system is far away from equilibrium, so choosing a larger C_{eq} would produce better agreement with the Fontorbe model at higher DSi concentrations and allow for the calculated free energy. Additionally, Maher (2011) details several ways in which C_{eq} could change depending on the conditions. For example, increasing PCO_2 would increase the concentration of DSi at equilibrium. However, if the Maher model assumes that all flow paths reach equilibrium, it is logical to use a concentration measured within the catchment; otherwise, applying the model would be of little relevance to the overall discussion on weathering controls.

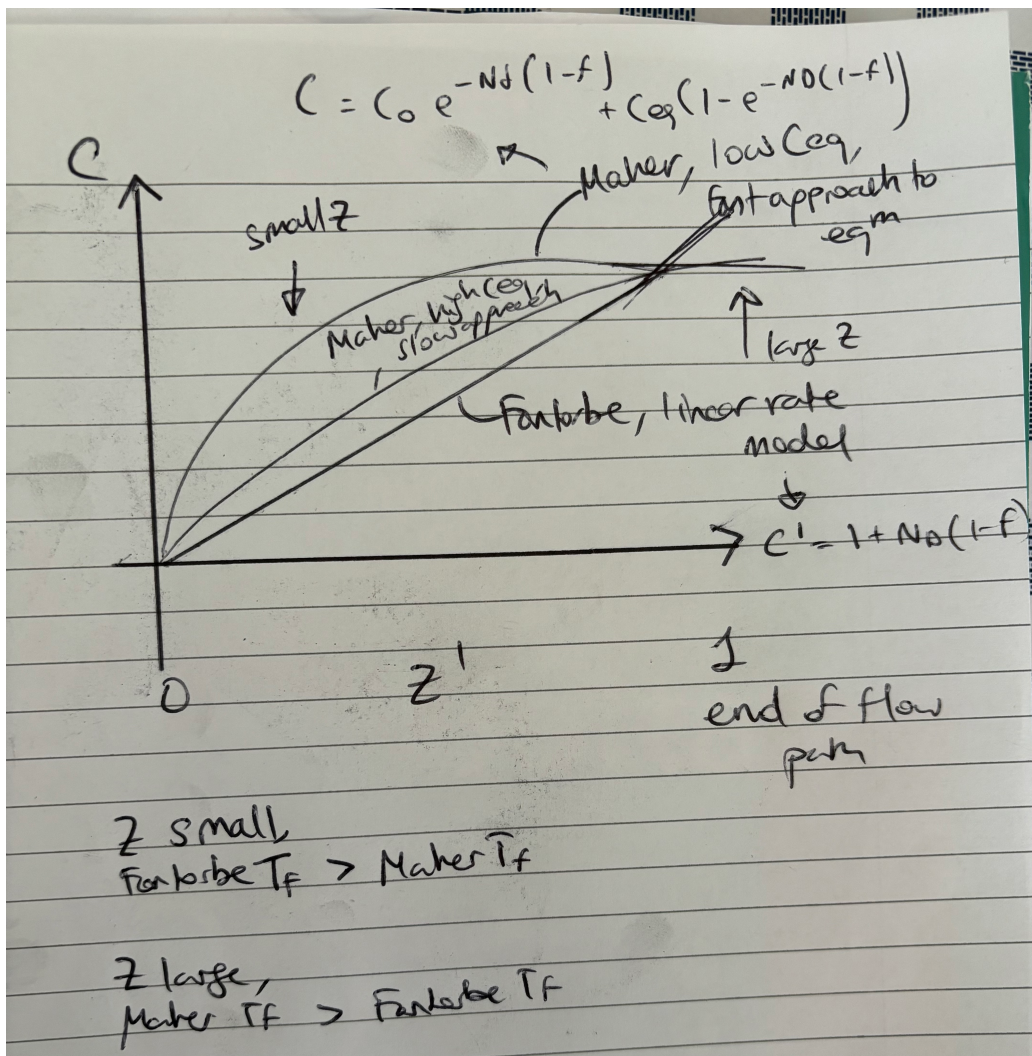


Figure 12: Comparison of how concentration changes with flow path length for the two models, and different equilibrium concentration

There is another pitfall related to the dependence of residence time on the concentration of DSi. As is apparent in Figures ?? ?? and Equations ??, the estimated residence time of both models is directly related to the concentration of DSi in the spring water. This is by design, however as expressed in Subsection 6.1 (ref), low DSi is not necessarily indicative of less reacted groundwater. As a result of this, there is the possibility that the estimated residence times act more as a lower bound. A better approach in a future study could use elemental ratios, for example Na/Si that has a known behaviour as the reaction progresses. Elemental ratios would also factor out dilution as a potential influencing factor.

6.5 Significance of Free Energy for Reaction Rate

Figure 11 suggests that the system is far away from equilibrium, but the reaction rate constant used in both models for all calculations is one that is only considered feasible when close to equilibrium (Kampman et al., 2014). Both the Maher and Fontorbe model predict residence times consistent with the gas ages obtained by Atwood et al. (2021); it is just the free energy of reaction that allows for the conclusion that the greatest control on weathering in the catchment is temperature and not hydrology. In systems far from equilibrium, the reaction rate constant has been suggested to be much larger than those used in the models (Kampman et al., 2014). However, if the reaction rate is increased, the residence times predicted by the models will decrease. This is because the rate of reaction is inversely proportional to the residence time, as seen in the equations in Table 5. Reaction rate constants that are suggested to be far from equilibrium in Kampman et al. (2014) are laboratory-derived rates, and four orders of magnitude higher than those used in this study. Using these rates for the models predicts residence times in the range of 1-10 days. Under the assumption that the rates displayed Kampman et al. (2014) are accurate for systems far away from equilibrium, the results no longer agree with Atwood et al. (2021). Under these circumstances, then, the Maher and Fontorbe models are less likely to be appropriate for use in discussing weathering controls.

There are, however, counterarguments to this. Firstly, Kampman et al. (2014) investigates a catchment draining a different lithology, under different pH and pCO₂ conditions than Melamchi. Secondly, the reaction rate constants reported at far from equilibrium free energies are laboratory-calculated, at different conditions to both this study and Kampman et al. (2014). As discussed in the Introduction (ref), field derived reaction rate constants are often found to be lower than those measured in the lab. It is therefore unclear whether the k- ΔG relationship suggested in Kampman et al. (2014) is applicable to Melamchi, or natural catchments in general. In other words, in the absence of field-derived reaction rate constants in far from equilibrium settings, there is little evidence to suggest that the rate constants used in this study, and the models' calculated residence times are incor-

rect. This study therefore suggests that the Maher and Fontorbe models are appropriate for use in natural catchments like Melamchi, and that the greatest control on weathering is temperature.

7 Conclusions and Future Work

Talk about using element ratios, and also isotope tracers eg Jotis, and also different reaction rates for forward and backward

References

- [1] Open-file report. Series: Open-File Report.
- [2] Sunil Acharya, Xiaoxin Yang, Tandong Yao, and Dibas Shrestha. Stable isotopes of precipitation in nepal himalaya highlight the topographic influence on moisture transport. 565:22–30.
- [3] Tirtha Raj Adhikari, Binod Baniya, QiuHong Tang, Rocky Talchabhadel, Manish Raj Gouli, Bhumi Raj Budhathoki, and Ram Prasad Awasthi. Evaluation of post extreme floods in high mountain region: A case study of the melamchi flood 2021 at the koshi river basin in nepal. 3(3):437–446.
- [4] Christoff Andermann, Laurent Longuevergne, Stéphane Bonnet, Alain Crave, Philippe Davy, and Richard Gloaguen. Impact of transient groundwater storage on the discharge of himalayan rivers. 5(2):127–132.
- [5] C. A. J. Appelo and Dieke Postma. Geochemistry, groundwater and pollution. CRC Press, 2nd ed., 5th corr. repr edition.
- [6] Abra Catherine Atwood. Critical zone response to perturbation: from mountain building to wildfire.
- [7] Binod Baniya, QiuHong Tang, Tirtha Raj Adhikari, Gang Zhao, Gebremedhin Gebremeskel Haile, Madan Sigdel, and Li He. Climate change induced melamchi extreme flood and environment implication in central himalaya of nepal. 120(12):11009–11029.
- [8] Paolo Benettin, Scott W. Bailey, John L. Campbell, Mark B. Green, Andrea Rinaldo, Gene E. Likens, Kevin J. McGuire, and Gianluca Botter. Linking water age and solute dynamics in streamflow at the hubbard brook experimental forest, NH, USA. 51(11):9256–9272.

- [9] Craig M Bethke. GEOCHEMICAL AND BIOGEOCHEMICAL REACTION MODELING, second edition.
- [10] M.J. Bickle, E. Tipper, A. Galy, H. Chapman, and N. Harris. On discrimination between carbonate and silicate inputs to himalayan rivers. 315(2):120–166.
- [11] Bodo Bookhagen and Douglas W. Burbank. Toward a complete himalayan hydrological budget: Spatiotemporal distribution of snowmelt and rainfall and their impact on river discharge. 115:2009JF001426.
- [12] Jesús Carrera, Maarten W. Saaltink, Joaquim Soler-Sagarra, Jingjing Wang, and Cristina Valhondo. Reactive transport: A review of basic concepts with emphasis on biochemical processes. 15(3):925.
- [13] Mingkun Chen, Lei Gong, Jacques Schott, Peng Lu, Kaiyun Chen, Honglin Yuan, Jian Sun, Si Athena Chen, John Apps, and Chen Zhu. Coupled feldspar dissolution and secondary mineral precipitation in batch systems: 6. labradorite dissolution, calcite growth, and clay precipitation at 60 °c and pH 8.2–8.4. 390:181–198.
- [14] Christian David, Teng-Fong Wong, Wenlu Zhu, and Jiaxiang Zhang. Laboratory measurement of compaction-induced permeability change in porous rocks: Implications for the generation and maintenance of pore pressure excess in the crust. 143(1):425–456.
- [15] Megh Raj Dhital. Geology of the Nepal Himalaya. Regional Geology Reviews. Springer International Publishing.
- [16] Jennifer L. Druhan and Kate Maher. The influence of mixing on stable isotope ratios in porous media: A revised rayleigh model. 53(2):1101–1124.
- [17] Benoît Dubacq. Thermodynamics of ordering and mixing in plagioclase feldspars: atomistic modelling in favour of landau theory. 177(10):102.
- [18] Guillaume Fontorbe, Christina L. De La Rocha, Hazel J. Chapman, and Michael J. Bickle. The silicon isotopic composition of the ganges and its tributaries. 381:21–30.

- [19] J. Gaillardet, B. Dupré, P. Louvat, and C.J. Allègre. Global silicate weathering and CO₂ consumption rates deduced from the chemistry of large rivers. 159(1):3–30.
- [20] Albert Galy, Christian France-Lanord, and Louis A Derry. The strontium isotopic budget of himalayan rivers in nepal and bangladesh. 63(13):1905–1925.
- [21] R.B. Georg, B.C. Reynolds, A.J. West, K.W. Burton, and A.N. Halliday. Silicon isotope variations accompanying basalt weathering in iceland. 261(3):476–490.
- [22] R.B. Georg, B.C. Reynolds, A.J. West, K.W. Burton, and A.N. Halliday. Silicon isotope variations accompanying basalt weathering in iceland. 261(3):476–490.
- [23] Jon K. Golla, Marie L. Kuessner, Michael J. Henehan, Julien Bouchez, Daniella M. Rempe, and Jennifer L. Druhan. The evolution of lithium isotope signatures in fluids draining actively weathering hillslopes. 567:116988.
- [24] Bradley W. Goodfellow, George E. Hilley, Samuel M. Webb, Leonard S. Sklar, Seulgi Moon, and Christopher A. Olson. The chemical, mechanical, and hydrological evolution of weathering granitoid. 121(8):1410–1435.
- [25] Emma L. S. Graf, Hugh D. Sinclair, Mikael Attal, Boris Gailleton, Basanta Raj Adhikari, and Bishnu Raj Baral. Geomorphological and hydrological controls on sediment export in earthquake-affected catchments in the nepal himalaya.
- [26] Danielle K. Hare, Ashley M. Helton, Zachary C. Johnson, John W. Lane, and Martin A. Briggs. Continental-scale analysis of shallow and deep groundwater contributions to streams. 12(1):1450.
- [27] Madeline M Hille. The orographic influence on storm variability, extreme rainfall characteristics and rainfall-triggered landsliding in the central nepalese himalaya.
- [28] T.J. B. Holland and R. Powell. An improved and extended internally consistent thermodynamic dataset for phases of petrological interest, involving a new equation of state for solids: THERMODYNAMIC DATASET FOR PHASES OF PETROLOGICAL INTEREST. 29(3):333–383.

- [29] L. Illien, C. Andermann, C. Sens Schönfelder, K. L. Cook, K. P. Baidya, L. B. Adhikari, and N. Hovius. Subsurface moisture regulates himalayan groundwater storage and discharge. 2(2):e2021AV000398.
- [30] Scott Jasechko. Global isotope hydrogeology review. 57(3):835–965.
- [31] Scott Jasechko. Partitioning young and old groundwater with geochemical tracers. 427:35–42.
- [32] A. Joshua West, Mike J. Bickle, Rob Collins, and James Brasington. Small-catchment perspective on himalayan weathering fluxes. 30(4):355.
- [33] Pratik Kad and Kyung Ja Ha. Recent tangible natural variability of monsoonal orographic rainfall in the eastern himalayas. 128(22):e2023JD038759.
- [34] Niko Kampman, Mike Bickle, John Becker, Nelly Assayag, and Hazel Chapman. Feldspar dissolution kinetics and gibbs free energy dependence in a CO₂-enriched groundwater system, green river, utah. 284(3):473–488.
- [35] D. B. Kattel, T. Yao, K. Yang, L. Tian, G. Yang, and D. Joswiak. Temperature lapse rate in complex mountain terrain on the southern slope of the central himalayas. 113(3):671–682.
- [36] Julia L. A. Knapp, Colin Neal, Alessandro Schlumpf, Margaret Neal, and James W. Kirchner. New water fractions and transit time distributions at plynlimon, wales, estimated from stable water isotopes in precipitation and streamflow. 23(10):4367–4388.
- [37] Alasdair C.G. Knight, Emily I. Stevenson, Luke Bridgestock, J. Jotautas Baronas, William J. Knapp, Basanta Raj Adhikari, Christoff Andermann, and Edward T. Tipper. The impact of adsorption–desorption reactions on the chemistry of himalayan rivers and the quantification of silicate weathering rates. 641:118814.
- [38] Lee R. Kump, Susan L. Brantley, and Michael A. Arthur. Chemical weathering, atmospheric CO₂, and climate. 28(1):611–667.

- [39] Başak Kısakürek, Rachael H. James, and Nigel B.W. Harris. Li and δ^{7Li} in himalayan rivers: Proxies for silicate weathering? 237(3):387–401.
- [40] K. Maher. The dependence of chemical weathering rates on fluid residence time. 294(1):101–110.
- [41] K. Maher. The role of fluid residence time and topographic scales in determining chemical fluxes from landscapes. 312(1):48–58.
- [42] K. Maher and C. P. Chamberlain. Hydrologic regulation of chemical weathering and the geologic carbon cycle. 343(6178):1502–1504.
- [43] K. Maher and C. P. Chamberlain. Hydrologic regulation of chemical weathering and the geologic carbon cycle. 343(6178):1502–1504.
- [44] Kate Maher, Carl I. Steefel, Art F. White, and Dave A. Stonestrom. The role of reaction affinity and secondary minerals in regulating chemical weathering rates at the santa cruz soil chronosequence, california. 73(10):2804–2831.
- [45] Katharine Maher, Donald J. DePaolo, and Jo Chiu-Fang Lin. Rates of silicate dissolution in deep-sea sediment: In situ measurement using $^{234}U/^{238}U$ of pore fluids. 68(22):4629–4648.
- [46] Odin Marc, Robert Behling, Christoff Andermann, Jens M. Turowski, Luc Illien, Sigrid Roessner, and Niels Hovius. Long-term erosion of the nepal himalayas by bedrock landsliding: the role of monsoons, earthquakes and giant landslides. 7(1):107–128.
- [47] James L. McCallum, Peter G. Cook, and Craig T. Simmons. Limitations of the use of environmental tracers to infer groundwater age. 53:56–70.
- [48] K. J. McGuire, J. J. McDonnell, M. Weiler, C. Kendall, B. L. McGlynn, J. M. Welker, and J. Seibert. The role of topography on catchment scale water residence time. 41(5):2004WR003657.
- [49] William G. Medwedeff, Marin K. Clark, Dimitrios Zekkos, A. Joshua West, and Deepak Chamlagain. Near surface geomechanical properties and weathering char-

acteristics across a tectonic and climatic gradient in the central nepal himalaya. 127(2):e2021JF006240.

- [50] Jeeban Panthi, Piyush Dahal, Madan Shrestha, Suman Aryal, Nir Krakauer, Soni Pradhanang, Tarendra Lakhankar, Ajay Jha, Mohan Sharma, and Ramchandra Karki. Spatial and temporal variability of rainfall in the gandaki river basin of nepal himalaya. 3(1):210–226.
- [51] Michelle A. Pedrazas, W. Jesse Hahm, Mong Han Huang, David Dralle, Mariel D. Nelson, Rachel E. Breunig, Kristen E. Fauria, Alexander B. Bryk, William E. Dietrich, and Daniella M. Rempe. The relationship between topography, bedrock weathering, and water storage across a sequence of ridges and valleys. 126(4):e2020JF005848.
- [52] Jay Quade, Nathan English, and Peter G DeCelles. Silicate versus carbonate weathering in the himalaya: a comparison of the arun and seti river watersheds. 202(3):275–296.
- [53] Kevin Roback, Marin K. Clark, A.Joshua West, Dimitrios Zekkos, Gen Li, Sean F. Gallen, Deepak Chamlagain, and Jonathan W. Godt. The size, distribution, and mobility of landslides caused by the 2015 mw7.8 gorkha earthquake, nepal. 301:121–138.
- [54] Joaquim Soler-Sagarra, Maarten W. Saaltink, Francesca De Gaspari, Albert Nardi, and Jesús Carrera. Water mixing approach (WMA) for reactive transport modeling.
- [55] Matthias Sprenger, Christine Stumpp, Markus Weiler, Werner Aeschbach, Scott T. Allen, Paolo Benettin, Maren Dubbert, Andreas Hartmann, Markus Hrachowitz, James W. Kirchner, Jeffrey J. McDonnell, Natalie Orlowski, Daniele Penna, Stephan Pfahl, Michael Rinderer, Nicolas Rodriguez, Maximilian Schmidt, and Christiane Werner. The demographics of water: A review of water ages in the critical zone. 57(3):800–834.
- [56] R. F. Stallard and J. M. Edmond. Geochemistry of the amazon: 2. the influence of geology and weathering environment on the dissolved load. 88:9671–9688.

- [57] Philip A. E. Pogge Von Strandmann, Mathieu Dellinger, and A. Joshua West. Lithium Isotopes: A Tracer of Past and Present Silicate Weathering. Cambridge University Press, 1 edition.
- [58] Nicholas E. Thiros, Erica R. Siirila Woodburn, P. James Dennedy Frank, Kenneth H. Williams, and W. Payton Gardner. Constraining bedrock groundwater residence times in a mountain system with environmental tracer observations and bayesian uncertainty quantification. 59(2):e2022WR033282.
- [59] Edward T Tipper. The isotopic fingerprint of calcium and magnesium: from the alteration of the continental crust to global budgets.
- [60] Edward T. Tipper, Mike J. Bickle, Albert Galy, A. Joshua West, Catherine Pomiès, and Hazel J. Chapman. The short term climatic sensitivity of carbonate and silicate weathering fluxes: Insight from seasonal variations in river chemistry. 70(11):2737–2754.
- [61] Rong Wen, LiDe Tian, YongBiao Weng, ZhongFang Liu, and ZhongPing Zhao. The altitude effect of δ 18O in precipitation and river water in the southern himalayas. 57(14):1693–1698.
- [62] A West, A Galy, and M Bickle. Tectonic and climatic controls on silicate weathering. 235(1):211–228.
- [63] A. J. West, M. Arnold, G. Aumaître, D. L. Bourlès, K. Keddadouche, M. Bickle, and T. Ojha. High natural erosion rates are the backdrop for present-day soil erosion in the agricultural middle hills of nepal. 3(3):363–387.
- [64] Art F. White, Alex E. Blum, Marjorie S. Schulz, Tom D. Bullen, Jennifer W. Harden, and Maria L. Peterson. Chemical weathering rates of a soil chronosequence on granitic alluvium: I. quantification of mineralogical and surface area changes and calculation of primary silicate reaction rates. 60(14):2533–2550.
- [65] Art F White and Susan L Brantley. The effect of time on the weathering of silicate minerals: why do weathering rates differ in the laboratory and field? 202(3):479–506.

- [66] John A Wojtowicz. The thermodynamic basis of the saturation index.
- [67] Bing Xu, Aihong Xie, and Jiangping Zhu. Can water vapor transport over the himalayas above 8000 m asl?—a case study on mt. everest. 14(11):1671.

Appendix 1: Rain and Hydrothermal Correction Equations

Spring water is corrected for rain input according to the average concentration for the closest rain sample collected in this field season. To remove the contribution of the rain the following formula is used for any element X:

$$[X]_{rain-corrected} = [X]_{river} - (Cl_{river} - Cl_{river}^*) \frac{[X]_{rain}}{Cl_{rain}} \quad (16)$$

$$Cl_{river}^* = Cl_{river} - Cl_{rain}; \quad \text{if } Cl_{river} > Cl_{rain} \quad (17)$$

Where $[Cl]_{river}^*$ is calculated by subtracting the concentration of chloride in the rain from that in the river (Tipper et al, 2006). Cl^* is taken to be zero if the concentration of chloride in the rain is greater than concentration of river. Evapotranspiration is not considered by this model, and studies which show that it plays a minor role, accounting for less than 10% of the hydrological budget in the Himalayas (Andermann et al (2012); Bookhagen and Burbank, 2010). In those cases where Cl^* is not zero then, a primary rain correction is simply:

$$[X]_{rain-corrected} = [X]_{river} - [X]_{rain} \quad (18)$$

Once the samples have been corrected for rain input, the remaining $[Cl]^-$ is assumed to be derived from hydrothermal springs encountered in the flow path. This is likely to be the case in one of the southern traverses (Traverse 2) in Melamchi which display high chloride concentrations even after the cyclic correction. Hence, the sample with the highest $[Cl]^-$ is used to correct:

$$[X]_{hydrothermal-corrected} = [X]_{rain-corrected} - \frac{[X]}{[Cl]_{highest-Cl}} * [Cl]_{rain-corrected} \quad (19)$$

This ensures that all chloride in the corrected sample is removed. The correction uses ionic ratios from the most concentrated water source, which acts as a proxy for the sediment imparting its signature. In this way, the correction does not affect samples which do not have high Cl (and hence do not have a large hydrothermal contribution), but does decrease the concentration of ions for those that do. In the following sections, samples are plotted with the evaporite correction applied where possible. Only in those cases where no chloride was measured is the evaporite correction not applied.

Appendix 2: Derivation of Reactive Transport Models

Fontorbe et al. (2013) Model Derivation

This model investigates silicon isotopic composition in the Ganges River, assuming constant reaction rates along flow paths. The model is initially built to predict Si concentrations, but in this study it is adapted to calculate residence times.

The first-order differential equation governing transport and reaction is given as:

To simplify, we introduce non-dimensional variables:

Rewriting Equation 21 using these new variables:

$$\phi \frac{\partial C}{\partial t} = -\omega \phi \frac{\partial C}{\partial z} + R_n(1-f) \quad (20)$$

$$C' = \frac{C}{C_o}, \quad z' = \frac{z}{h}, \quad t' = \frac{t\omega}{h} \quad (21)$$

The Damköhler number (N_D) describes the relative importance of kinetic vs transport-controlled settings (Bethke, 2008):

$$N_D = \frac{R_n h}{\phi C_o \omega} \quad (23)$$

Assuming a quasi-stationary state ($\partial C'/\partial t' = 0$), we get:

$$C' = 1 + z' N_D (1-f) \quad (24)$$

At the end of the flow path ($z = h, z' = 1$), this simplifies to:

$$N_D = \frac{C' - 1}{1 - f} \quad (25)$$

The residence time of water along the flow path is:

$$T_f = \frac{h}{\omega} \quad (26)$$

At the end of the flow path:

$$\frac{R_n h}{\phi C_o \omega} = \frac{C' - 1}{1 - f} \quad (27)$$

$$\frac{R_n T_f}{\phi C_o} = \frac{C' - 1}{1 - f} \quad (28)$$

Solving for residence time T_f and reaction rate R_n :

$$T_f = \frac{(C - C_o)\phi}{(1 - f)R_n} \quad (29)$$

C is the concentration at the end of the flow path, which is taken to be equal to the concentration of each spring, assuming each spring represents a unique flow path. Note that given these units, the calculation gives time in 10^{-3} s. This is converted to years for practical use.

Fontorbe			
Parameter	Definition	Units	Formula (Value)
ϕ	Porosity	-	0.1*
ω	Fluid velocity	m/s	Variable
h	Length of flow path	m	Variable
C	Concentration end of flow path	$\mu\text{mol/L}$	Variable
C_0	Initial concentration	$\mu\text{mol/L}$	Rain Input
f	Fraction reprecipitated	-	0.5*
N_D	Damkohler Number	-	$N_D = \frac{R_n h}{\phi C_0 \omega}$
T_f	Residence time	s	$T_f = \frac{h}{\omega \phi}$
R_n	Reaction rate	$\text{mol}/\text{m}^3/\text{s}$	$\rho \cdot 10^6 \cdot k \cdot S \cdot X$
k	Reaction rate constant	$\text{mol}/\text{m}^2/\text{s}$	10^{-15*}
S	Specific surface area	m^2/g	0.1*
ρ	Plagioclase density	g/cm^3	2.7*
X	Volume fraction of mineral in rock	$g_{\text{min}}/g_{\text{rock}}$	0.2*

Table 6: Key parameters and definitions for the Fontorbe model. Starred terms are values used for calculation.

Maher (2011) Model Derivation

This model describes a reaction-based approach to solute transport, following Maher and Chamberlain (2014). Maher (2011) suggests a dissolution rate law which decreases linearly to zero at equilibrium. The first-order differential equation governing transport and reaction is:

$$\frac{dC}{dt} = -\frac{q}{\theta} \frac{dC}{dz} + \sum_i \mu_i R_{d,i} \left(1 - \left(\frac{C}{C_{eq}} \right)^{n_i} \right)^{m_i} - \sum_i \mu_i R_{p,i} \left(1 - \left(\frac{C}{C_{eq}} \right)^{n_i} \right)^{m_i} \quad (30)$$

Where C is the concentration, q is the fluid flux, θ is the volumetric water content, z is the position along the flow path, μ is the stoichiometric coefficient, R is the rate of reaction for dissolution and precipitation respectively, C_{eq} is the equilibrium concentration, and n and m are non-linear parameters (Maher and Chamberlain, 2014). Defining the net reaction rate for a set of packets i :

$$R_n = \sum_i \mu_i R_{d,i} - \sum_i \mu_i R_{p,i} \quad (31)$$

Maher and Chamberlain describe that the reaction rate decreases linearly with approach to equilibrium.

$$\frac{dc}{dt} = R_n \left(1 - \frac{C}{C_{eq}} \right) \quad (32)$$

Solving for C , following Maher and Chamberlain (2014):

$$C = C_0 \exp \left(-\frac{R_n \theta h}{q C_{eq}} \right) + C_{eq} \left(1 - \exp \left(-\frac{R_n \theta h}{q C_{eq}} \right) \right) \quad (33)$$

The residence time T_f is defined as:

$$T_f = \frac{h\phi}{q} \quad (34)$$

Thus, at residence time T_f :

$$c(T_f) = c_0 \exp \left(-\frac{R_n T_f}{c_{eq}} \right) + c_{eq} \left(1 - \exp \left(-\frac{R_n T_f}{c_{eq}} \right) \right) \quad (35)$$

Following Maher and Chamberlain (2014), this can be rewritten as:

$$C = \frac{C_0}{1 + \tau D_w / q} + C_{eq} \frac{\tau D_w / q}{1 + \tau D_w / q} \quad (36)$$

Where:

$$\tau = e^2; \quad D_w = \frac{h\theta R_n}{C_{eq}} \quad (37)$$

Rewriting the equation:

$$C = \frac{C_0 + C_{\text{eq}} \cdot T_f (e^2 \cdot R_n / C_{\text{eq}})}{1 + T_f (e^2 \cdot R_n / C_{\text{eq}})} \quad (38)$$

Solving for residence time T_f :

$$T_f = \frac{C_{\text{eq}} \cdot (C - C_0)}{e^2 R_n (C_{\text{eq}} - C)} \quad (39)$$

Note that given these units, the calculation gives time in 10^{-3} s. This is converted to years for practical use. Also note the e^2 term is used because the Maher model considers all paths as if they approach equilibrium.

Maher			
Parameter	Definition	Units	Formula (Value)
ϕ	Porosity	-	0.1*
h	Length of flow path	m	Variable
q	Flow rate	m/s	Variable
C_{eq}	Equilibrium concentration	$\mu\text{mol/L}$	Max Catchment
C_0	Initial concentration	$\mu\text{mol/L}$	Rain Input
R_n	Net reaction rate	mol/L/s	$\rho \cdot 10^6 \cdot k \cdot S \cdot X$
ρ	Plagioclase density	g/cm^3	2.7*
k	Reaction rate constant	$\text{mol/m}^2/\text{s}$	10^{-15*}
S	Specific surface area	m^2/g	0.1*
X	Volume fraction of mineral in rock	$g_{\text{min}}/g_{\text{rock}}$	0.2*
τ	Scaling factor	-	$\tau = e^2$
D_w	Damkohler Coefficient	m^2/s	$D_w = \frac{L\phi R_n}{C_{\text{eq}}}$
T_f	Residence time	s	$T_f = \frac{h\phi}{q}$

Table 7: Key parameters and definitions for the Maher model. Starred terms are values used for calculation.